What caused the interdecadal shift of the ENSO impact on dust mass concentration over northwestern South Asia?

Lamei Shi [1, 2], Jiahua Zhang [1, 2], Da Zhang [1, 2], Jingwen Wang [1, 2], Xianglei Meng[2], Yuqin Liu[3], Fengmei Yao [2]

[1] Key Laboratory of Digital Earth Science, Aerospace Information Research Institute, Chinese Academy of Sciences, Beijing 100094, China

[2] College of Earth and Planetary Sciences, University of Chinese Academy of Sciences, Beijing 101407, China

[3] Key Laboratory of Urban Environment and Health, Institute of Urban Environment, Chinese Academy of Sciences, Xiamen 361021, China

Correspondence to: Jiahua Zhang (zhangjh@radi.ac.cn)

Abstract. The changes of large-scale circulation, especially El Niño-Southern Oscillation (ENSO), have significant impacts on dust activities over the dust source and downwind regions. However, these impacts present an interdecadal pattern and it remains less clear that which factors lead to the interdecadal variability of the ENSO impact on dust activities over the northwestern South Asia, although previous studies have discussed the response of the interannual dust activities over the northwestern South Asia to the ENSO circle. Based on the linear regression model and MERRA-2 atmospheric aerosol reanalysis data, this study investigated the interdecadal variability of the ENSO impact on dust activities as well as the associated possible atmospheric drivers under two different warming phases over the northwestern South Asia. Results indicated that the relationship between ENSO and Dust Column Mass Density (DUCMASS) experienced an obvious shift from the accelerated global warming period (1982–1996) to the warming hiatus period (2000–2014). The change of Atlantic and Indian ocean sea surface temperature anomaly (SSTA) pattern weakened the impact of ENSO on dust activities over the northwestern South Asia during 1982–1996, while the change of PDO strengthened ENSO's effect when it was in phase with ENSO. Both the Atlantic and Indian Ocean SSTA patterns were modulated by the duration of ENSO events (i.e., continuing and emerging ENSO). This study provides new sights to numerical simulation involving the influence of atmospheric teleconnections on the variability of dust activities and their influence mechanisms.

Keywords: Surface dust mass concentration; ENSO–DUCMASS relationship; interdecadal change;

30   large-scale atmospheric circulation; northwestern South Asia

31   **1 Introduction**

32   Dust aerosols are attracting an increasing concern due to its adverse impacts on human health (Chen

33   et al., 2004; Bozlaker et al., 2013; Erel et al., 2006; Kaiser and Granmar, 2005; Poulsen et al., 1995;

34   Sanchez de la Campa et al., 2013; Schulz et al., 2012) and environmental problems (Avila, 1998; Razakov

35   and Kosnazarov, 1996; Behrooz et al., 2017). Dust aerosols can also influence the earth's radiation budget

36   balance and climate change through direct and indirect effects (Mahowald et al., 2014; Miller and Tegen,

37   1998). Dust aerosols can reflect incoming solar radiation and cool the surface, which is known as the

38   direct effects (Mahowald et al., 2006; Tegen et al., 1996); they can also affect the cloud droplet size,

39   cloud albedo and lifespan by forming into cloud condensation nuclei and ice nuclei, which is known as

40   the indirect effects (Hansen et al., 1997). The Northwest Indian subcontinent, which is the most arid and

41   semiarid area of South Asia, suffers heavy and frequent dust storms in summer due to extremely dry

42   climate and strong winds (Jin and Wang, 2018). Those dusts can travel long-distance to North India and

43   the Arabian Sea, degrading air quality (Mahowald et al., 2010) and modifying ocean biogeochemistry

44   processes (Richon et al., 2018; Singh et al., 2008). Particularly, dust aerosols can change local radiation

45   budget, circulations, and Indian summer monsoon rainfall through absorption and scattering of solar

46   radiation (Wu et al., 2018; Jin et al., 2021; Mahowald et al., 2006; Tegen et al., 1996). The mineral dust

47   over the northwestern South Asia is closely associated with the long-term variation of global climate

48   (Bollasina et al., 2011; Jin et al., 2018; Banerjee et al., 2019). To better understand such feedback, and

49   give early warning to reduce disasters and losses caused by dust events, it is important to find out the

50   controlling factors of the Dust Column Mass Density (DUCMASS) and its long-term variation.

51   ENSO, as a periodic fluctuation in sea surface temperature (SST) and the air pressure across the

52   equatorial Pacific Ocean, is as the primary large-scale driver of dust loading over the global dust source

53   region (Trenberth et al., 2014). Prospero and Nees (1986) found that ENSO-related large-scale

54   atmospheric circulation changes led to the increase in winter dust concentration over North Africa. Xi

55   and Sokolik (2016a) indicated that in La Niña years, the precipitation and soil moisture over Central Asia

56   decreased and caused poor vegetation conditions and heavy drought conditions, which strengthened dust

57   activities. Yu et al. (2015b) suggested that La Niña events provided favorable conditions for dust

58   activities over Saudi Arabia. However, Banerjee et al. (2016) proposed that the low-level southwesterly

59   winds and high-level westerly winds accompanied with La Niña events were the main factor that

60   contributed to the elevated dust levels over the Arabia Peninsula. Abish and Mohanakumar (2013)

61   pointed out that strengthened westerly circulation related with El Niño increased the dust transmission

62   from the Middle East to the Indian subcontinent. Simultaneously, the impacts of ENSO on dust activities

63   were also modulated by other atmospheric factors, e.g., PDO could strengthen the effect of ENSO when

64   it was in phase with ENSO (He et al., 2013; Wang et al., 2008; Wang et al., 2014); the spring dust index

65   over the northern China in the years when negative AO and El Niño occurred synchronously was

66   significantly higher than that in the years when positive AO and La Niña were concurrent (Liu et al.,

67   2020; Lee et al., 2015); IOD could also influence the dust activities over the northwestern Indian ocean

68   by adjusting the El Niño related water vapor conditions (Banerjee and Kumar, 2016).

69   ENSO exhibits profound impacts on the global climate. Nevertheless, the Earth climate is varying

70   and ENSO, including its feedback and influences on the changing global climate, also experience

71   significant changes (Yang and Jiang, 2014; Yuan and Yang, 2012; Weng et al., 2007; Weare et al., 1976;

72   Yu and Kao, 2007; Ashok et al., 2007). In the mid-1970s, an interdecadal climate regime shift was

73   observed in the large-scale boreal winter circulation pattern over the North Pacific (Graham, 1994; Nitta

74   and Yamada, 1989; Trenberth and Hurrell, 1994). Another remarkable climate change was observed in

75   the early 21st century, i.e., an accelerated global warming prevailed before late 1990s and a warming

76   hiatus dominated after that (Easterling and Wehner, 2009; Fyfe et al., 2011, 2013). After 2013, the global

77   warming hiatus came to an end due to a persistent warm condition over the equatorial Pacific between

78   Mar. 2014 and May 2016 (Hu and Fedorov, 2017). Concurrent with the Pacific climate shift, the large-

79   scale circulation pattern and their atmospheric teleconnection also exhibited an interdecadal change, e.g.,

80   the correlation between El Niño and rainfall over India turned to be insignificant from the late 1970s,

81   simultaneously, the relationship between ENSO and monsoon also weakened around this turning point

82   (Kumar et al., 1999). Two influence mechanisms were proposed to explain this weakened ENSO–

83   monsoon relationship. One was the varied location of Walker circulation that adjusted the monsoon

84   rainfall over Indian region, the other was the temperature change over Eurasia that modulated the land-

sea thermal gradient. Besides, the impact of Atlantic Ocean pattern on the monsoon circulation over the Indian Ocean became stronger since late 1970s as the influence of the tropical Pacific has reduced (Srivastava et al., 2019; Sabeerali et al., 2019; Kucharski et al., 2007). This in-turn impacted the circulation responsible for dust uplift and transport.

It was reported that the effect of ENSO on Indian summer monsoon rainfall (ISMR), which was an important modulator to DUCMASS, experienced a remarkable interdecadal change and many factors may cause this transition (Yang and Huang, 2021). Till now, the interdecadal variability in the links of DUCMASS over the northwestern South Asia with ENSO has not been fully investigated, as compared to the North African and West Asian counterpart (Yu et al., 2015). In addition, though many factors have been proved to influence the short-term (e.g., interannual scale) variation of the relationship between ENSO and dust activities over South Asia, their effects on the long-term (e.g., interdecadal scale) change are still unclear. Cai et al. (2014) pointed out that global warming will have a significant impact on ENSO. The extreme El Niño events will become more frequent under the changes of atmospheric convention in the next half of the 21st century. Thus, understanding the physical mechanism of the shifting ENSO–DUCMASS relationship is of profound implications for the forecast of dust trend in the future climate change scenario. This study aims to investigate the large-scale atmospheric factors that contribute to the interdecadal variability of the ENSO impact on DUCMASS over the northwestern South Asia.

The paper is organized in the following structure: section 2 describes the datasets and methods; section 3 presents factors that influence the interdecadal change of the relationship between DUCMASS and wintertime Niño-3 index; section 4 discusses the deficiency and prospect of this study, and the conclusions are given in section 5.

2 Data and methods

2.1 Study area

The main dust source over South Asia is a large arid region in the northwestern part of the Indian subcontinent, which stretches from India to Pakistan. Most of the dust aerosols over this region come from the Thar desert. The southeastern part of the Thar desert lies between the Aravalli Hills. The desert extends as far as the Punjab Plain in the north and northeast, the alluvial plains of the Indus River in the

112   west and northwest, and the Great Rann of Kutch along the western coast. The desert presents an

113   undulating surface, with high and low sand dunes separated by sandy plains and low barren hills. The

114   soils are mainly consisted by desert soils, red desertic soils, sierozems, the red and yellow soils of the

115   foothills, the saline soils of the depressions, and the lithosols (shallow weathered soils) and regosols (soft

116   loose soils) found in the hills. The subtropical desert climate here results from persistent high pressure

117   and subsidence. The prevailing southwest monsoon winds from Indian Ocean that bring rain to much of

118   the Indian subcontinent in summer tend to bypass the Thar to the east. The soils are generally infertile

119   and overblown with sand due to severe wind erosion (Augustyn et al., 2019). The amount of annual

120   rainfall in the desert is low, ranging from about 100 mm or less in the west to about 500 mm in the east.

121   Almost 90 % of the annual rainfall occurs in the season southwest monsoon, from July to September.

122   While the prevailing wind is dry northeast monsoon during other seasons. Dust storms and dust-raising

123   winds are common from May to July (Chauhan, 2003). Thus, the DUCMASS used in this study is

124   averaged from June to July and May is neglected to eliminate the disturbance of seasonal climatological

125   differences. Analysis is carried out over the dust source in the northwestern South Asia (65°–82° E, 24°–

126   32° N), as shown in Fig. 1. All variables involving spatial average are taken from this region unless stated

127   otherwise.
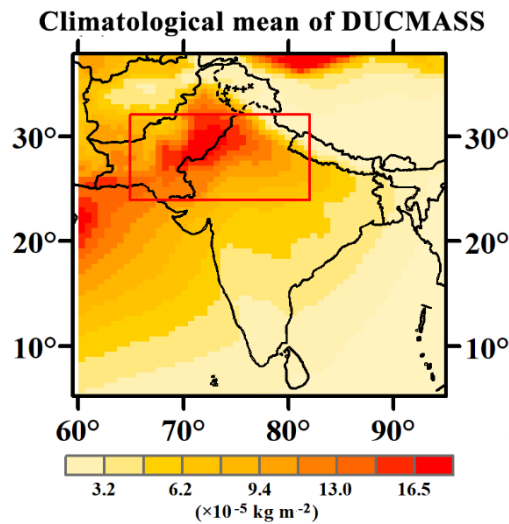
128
129   **Figure 1: Climatological mean DUCMASS over South Asia based on the MERRA-2 dataset. The dust source**
130   **over the northwestern South Asia is marked with red rectangle.**

131   **2.2 Datasets**

132   **2.2.1 Dust concentration**

133   Dust column mass density from 1982 to 2014 was obtained from the Modern-Era Retrospective

134   Analysis for Research and Applications, version 2 (MERRA-2). MERRA-2 is produced via the Goddard

135   Earth Observing System-Data Assimilation System (GEOS-DAS, version 5.12.4) based on GEOS-5

136   climate model and the Gridpoint Statistical Interpolation (GSI) analysis scheme (Gelaro et al., 2017).

137   Extensive satellite data are integrated into MERRA-2 to estimate dust concentration (Veselovskii et al.,

138   2018; Randles et al., 2017). The dust products were comprehensively validated using the results of

139   ground-based observation, satellite measurements, and numerical simulation (Buchard et al., 2017;

140   Randles et al., 2017). They have been widely applied to researches on global environment and climate

141   change (He et al., 2019; Randles et al., 2017). The variable "Dust Column Mass Density-PM$_{2.5}$"

142   (DUCMASS25) with a spatial resolution of 0.625°×0.5° (longitude×latitude) used in this study is from

143   the dataset of "tavgM_2d_aer_Nx". The time series of DUCMASS25 dataset was compared with that of

144   DUCMASS dataset, to find that the time series of DUCMASS25 and its association with Niño index

145   showed the same change pattern with that of DUCMASS. Only the results acquired by DUCMASS25

146   were presented in this study.

147   **2.2.2 Land and sea surface temperature**

148   To explore the possible influence of SST on the South Asian dust activity, we used three SST

149   datasets from 1981 to 2014 for comparison: (1) The National Oceanic and Atmospheric Administration

150   (NOAA) Extended Reconstructed SST (ERSST) version 5 (Huang et al., 2017) that is available at 2°×2°

151   spatial resolution is used for analysis, (2) Centennial in situ Observation-Based Estimates (COBE)

152   version 2 SST data at 1°×1° spatial resolution (Hirahara et al., 2014) and (3) Hadley Centre Global Sea

153   Ice and Sea Surface Temperature (HadISST1.1) dataset produced by the Met Office, starting from 1870

154   up to the present with a horizontal resolution of 1°×1° (Rayner et al., 2003). While the land-sea thermal

155   contrast was calculated from the Hadley Centre Climate Research Unit Temperature version 5.0.1.0

156   (HadCRUT5) data from 1981 to 2014, which is a blend of the Climatic Research Unit land-surface air

157   temperature dataset (CRUTEM5) and the Hadley Centre sea-surface temperature (HadSST4) dataset

158   (Osborn et al., 2021). The longitude and latitude of SST index involved in this study were shown in Table

159   1.

160 **Table 1: Longitude and latitude of SST index used in this study.**

Acronyms	Full Name	Longitude and Latitude	Involved Ocean
Niño-3	——	150°–90° W, 5° S–5° N	Pacific
Niño-3.4	——	170°–120° W, 5° S–5° N	Pacific
Niño-4	——	160° E–150° W, 5° S–5° N	Pacific
ASGI	Atlantic SSTA gradient index	North: 60°–30° W, 0–20° N South: 20° W–10° E, 0–20° S	Atlantic Ocean
TWISSTA	Tropical western Indian ocean SSTA	50°–70° E, 10° S–15° N	Indian Ocean
IOD	Indian Ocean Dipole	West: 50°–70° E, 10° S–10° N East: 90°–110° E, 10° S–0°	Indian Ocean
PDO	Pacific decadal oscillation	117.5° E–77° W, 20°–66.5° N	Pacific

161 **2.2.3 Large-scale climate indices**

162   Three monthly Niño indices Niño-3, Niño-3.4, and Niño-4 from 1981 to 2014, which monitor the

163 SST anomalies averaged across the eastern equatorial Pacific, Pacific from dateline to the South

164 American coast, and central equatorial Pacific, respectively, were used to analyze their links with

165 DUCMASS over the northwestern South Asia. Kinter et al. (2002) pointed out that Nov.–Jan. is the peak

166 season for El Niño/La Niña, thus the average Niño index from (–1) Nov. to (0) Jan. was used. Only one

167 Niño index that showed the highest correlation coefficient was retained in this study, i.e., Niño-3. The

168 time series of ENSO was represented by Niño-3 and Niño-3 also referred to ENSO. The large-scale

169 climate indices, such as PDO and IOD, was also used to explore the potential factors that contributed to

170 the interdecadal shift of ENSO–DUCMASS relationship. All those indices were from the Climate Predict

171 Center of National Oceanic and Atmospheric Administration (NOAA/CPC).

172 **2.3 Method**

173   In this study, we compared the impact of ENSO on DUCMASS over the northwestern South Asia

174 under two different warming epochs, and investigated the potential global change drivers to the shift of

175 ENSO–DUCMASS relationship. The global warming was separated into the accelerated warming period

176 from 1982 to 1996 (P1) and the warming hiatus period from 2000 to 2014 (P2). The year 2014 was added

177 to the warming hiatus period to keep the length of those two periods consistent. This classification was

178 not controversial since the ENSO year stated in this study spanned from antecedent November to current

179 January.

2.3.1 Contribution of factors to relationship

181 The contribution of X (Indian Ocean SSTA, Atlantic SSTA gradient index, and PDO) modifying

182 ENSO–DUCMASS relationship was defined as: sliding regression of X onto Niño-3 index multiplies by

183 sliding regression of DUCMASS onto X with Niño-3 removed (Yang and Huang, 2021).

2.3.2 Signal removal method

185 The ENSO signals were removed from the oceanic SSTA pattern when analyzing spatial coupling

186 and regression mode between the oceanic SSTA pattern and DUCMASS as well as local surface

187 conditions (precipitation, soil moisture, land cover, wind, etc). Simultaneously, the oceanic SSTA signals

188 were removed from ENSO when calculating the sliding correlation between ENSO and DUCMASS. In

189 this study, the residual time series based on the linear regression method were used to represent the ENSO

190 (or oceanic SSTA index)-independent components (Yang and Huang, 2021), as shown in Eq. (1):

$$\xi_{remove} = \xi - Z \times \frac{cov(\xi, Z)}{var(Z)} \tag{1}$$

191 Where ξ_{remove} is the time series of variable ξ with Z removed, ξ is the time series of original

192 variable, Z is the time series of related signal that needs to be removed, cov indicates the covariance

193 between two variables, and var indicates the variance of ENSO.

2.3.3 Coupled spatial pattern analysis

195 The maximum covariance analysis (MCA) is a useful tool for isolating the most coherent pairs of

196 spatial patterns and their associated time series by performing an eigenanalysis on the temporal

197 covariance matrix between two geophysical fields (Storch and Zwiers, 1999). The MCA method was

198 used to analyze the coupled patterns between DUCMASS and oceanic SSTA.

2.3.4 Definition of different types of ENSO

200 Following Yang and Huang (2021), the EM and CT ENSO were defined based on the three-month

running mean of the Niño-3 index. Two situations for the CT ENSO were considered, i.e., the slowly

decaying events and the developing events since the previous winter. For the slowly decaying situation,

a CT ENSO was identified when the average Niño-3 of (–1) Oct.–(0) Jan. was greater than 0.5 (below –

0.5) standard deviation (STD), became greater than 0.5 (below –0.5) STD in single month during (0)

Mar.–(0) May, and remained positive (negative) during (0) Jun.–(0) Sep.. For the developing events since

the previous winter, a CT ENSO was identified when the Niño-3 was greater than 0.75 (below –0.75)

STD in any month from (–1) Oct. to (0) May, accompanied by positive (negative) values for eight single

months, and the average Niño-3 of (0) Jun.–(0) Sep. was greater than 0.5 (below –0.5) STD. To acquire

more available samples in the study period, all the ENSO years that were not defined as CT ENSO were

identified as EM ENSO year in this study, which was different from Yang and Huang (2021). Based on

this definition, the CT El Niño years during 1982–2014 included 1982, 1983 and 1987; CT La Niña years

included 1984, 1985, 1989, 1996, 1999, 2000, and 2011; EM El Niño years included 1995, 1998, 2003,

2005, 2007, and 2010; EM La Niña years included 2008 and 2012.

In this study, "(0) month" represented the year concurrent with the year when DUCMASS was

acquired and "(–1) month" represented the preceding year.

3 Results

3.1 Observed interdecadal change of the impact of ENSO on DUCMASS

In the present study, we found that the DUCMASS–Niño-3 relationship experienced an interdecadal

transition at around 1999/2000. Based on the 15-year sliding correlation from 1982 to 2014 (Fig. 4 (a)),

the DUCMASS–Niño-3 relationship was weak before the early of 2000s and became stronger after that.

Specifically, the winter Niño-3 index ((–1) Nov.–(0) Jan.) presented a significant negative relation (R=–

0.68, p<0.01) with DUCMASS during 2000–2014 (P2), while no significant correlation (R=–0.41,

p>0.05) was observed in 1982–1996 (P1), as shown in Fig. 2.
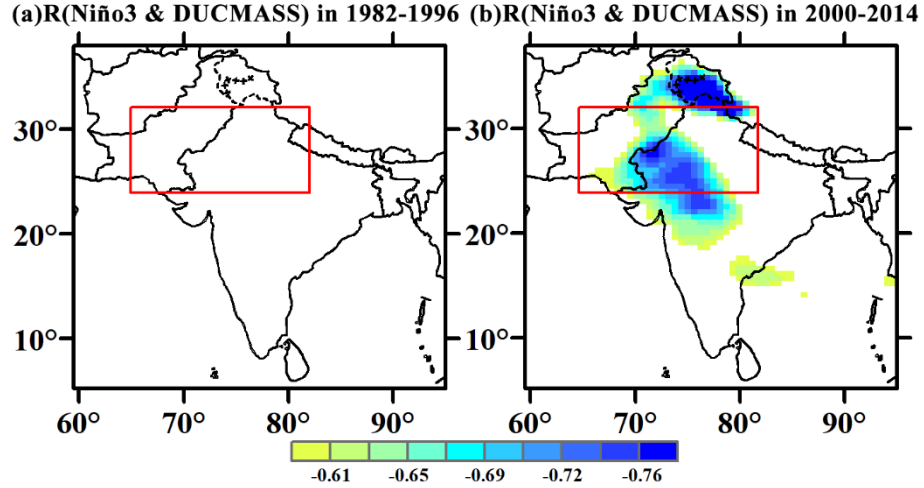
Figure 2: Correlation between Niño-3 index and DUCMASS over South Asia during (a) 1982–1996 and (b) 2000–2014. (Only correlations that passed the 99% confidence level were presented).

3.2 Factors influencing the interdecadal change of the impact of ENSO on DUCMASS

3.2.1 Tropical Atlantic SSTA pattern

With the global climate change observed in early 2000s, the ENSO-related tropical Atlantic SSTA experienced an obvious transition, i.e., from an Atlantic Niña pattern during 1982–1996 to an Atlantic Niño pattern during 2000–2014 (Fig. 3), which coincides with the findings of Yang and Huang (2021). The tropical Atlantic SSTA pattern was a crucial factor for the restoration of ENSO–ISMR relationship since the late 1990s (Yang and Huang, 2021), thus, it could also disturb the impact of ENSO on dust activities over the northwestern South Asia. In order to validate the connection between the Atlantic SSTA and the DUCMASS–Niño-3 relationship, an Atlantic SSTA gradient index (ASGI) was used to describe the SSTA pattern shift in the tropical Atlantic, which represented the difference of averaged SSTA between tropical North Atlantic and tropical South Atlantic (marked by two rectangles in Fig. 3). According to Tokinaga et al. (2019), the Atlantic Niña pattern develops and is most sensitive to ENSO in spring, thus the SST averaged from Mar. to May was used in this section.
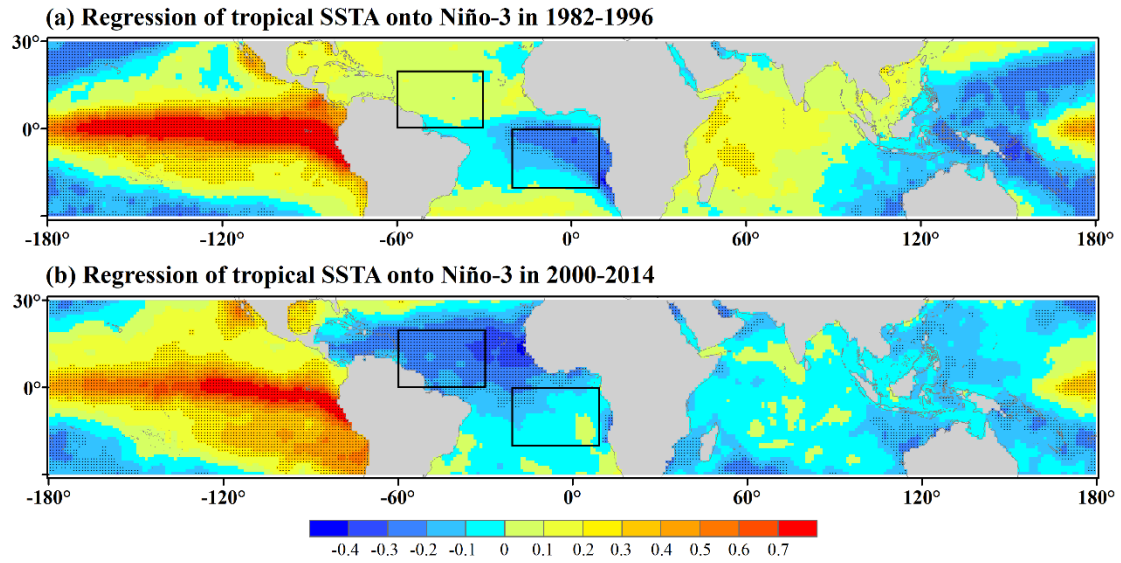
Figure 3: Regression of spring (Mar.–May) tropical SSTA onto Niño-3 index. Black rectangles denote the regions to define ASGI. The range of the upper one is 60–30° W, 0–20° N and that of the lower one is 20° W–10° E, 20–0° S. The black dots represent significance at ≥90 % confidence level. (Similar with Fig. 2 (c)–(d) of Yang and Huang (2021) but with different time spans)

The relationship between Niño-3 and DUCMASS witnessed a reversal at the early 2000s, simultaneously, the correlation between Niño-3 and ASGI exhibited the similar change. The correlation between Niño-3 and ASGI passed the 99% confidence level during P1, while it did not pass the 95% confidence level during P2, as shown in Fig. 4 (b). However, the correlation between Niño-3 and DUCMASS showed a contrary trend with a higher correlation coefficient appeared in P2. Figure 4 (a) showed that the DUCMASS–Niño-3 relationship was weakened when the ASGI signals were removed from Niño-3 index during P1, while during P2, the DUCMASS–Niño-3 relationship remained the same with or without the ASGI signals removed. In addition, the contribution of ASGI to the DUCMASS–Niño-3 relationship (Fig. 4 (c)) proved that during P1, ASGI weakened this relationship while no significant contribution was observed during P2. Thus, it is hypothesized that the strengthening (weakening) of the response of ASGI to Niño-3 weakened (strengthened) the impact of Niño-3 on DUCMASS during P1 (P2).

257
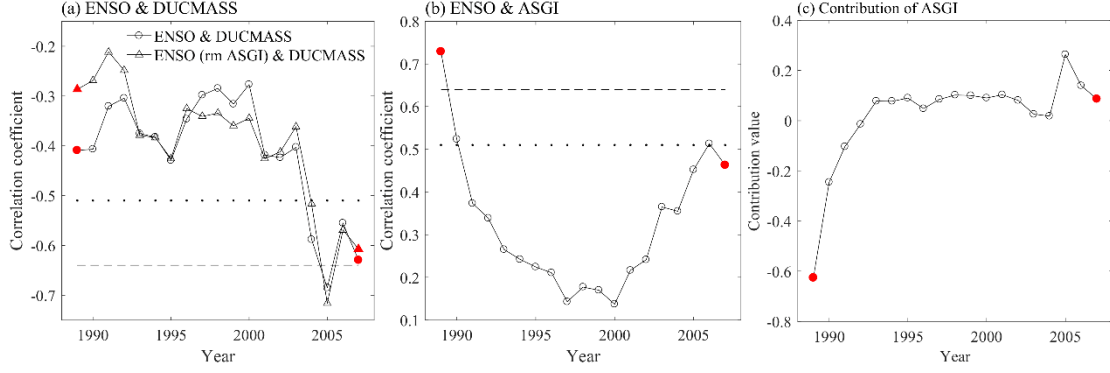
258 **Figure 4: (a) The 15-year sliding correlation between DUCMASS and Niño-3 with and without ASGI-related**

259 **signals removed; (b) 15-year sliding correlation between Niño-3 and ASGI; (c) Sliding contribution of ASGI**

260 **to DUCMASS–Niño-3 relationship. The two red filled markers represented the 15-year window spanning**

261 **from 1982 to 1996 and 2000 to 2014, respectively. The x-axis denotes the middle year of the period under**

262 **analysis.**

263
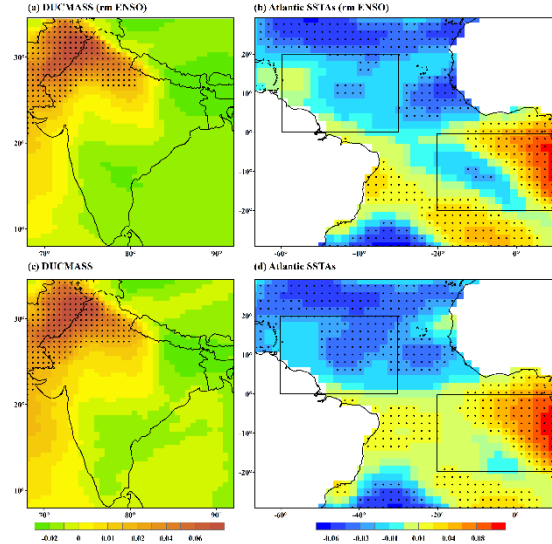
264 **Figure 5: Spatial correlation between spring (Mar.–May) tropical Atlantic SSTA and DUCMASS of the first**

265 **mode of the MCA analysis in 1982–2014. The first MCA mode of (a) the DUCMASS, and (b) the tropical**

266 **Atlantic SSTA with ENSO-related signals removed. (c)–(d) As in (a)–(b), but for the original series including**

267 **the ENSO signal. The black dots represent significance at ≥90 % confidence level.**

268   In order to validate the effect of Atlantic SSTA pattern on the DUCMASS–Niño-3 relationship, the

269 spatial coupling mode between DUCMASS and tropical Atlantic SSTA was explored. Figure 5 showed

270 that the negative ASGI, i.e., negative SST anomaly over the tropical North Atlantic and positive SST

271 anomaly over the tropical South Atlantic, was coupled with increased DUCMASS over the northern and

272 northwestern India. This pattern was not impacted by ENSO since the MCA results with ENSO-related

273 signals removed were similar with that including the ENSO-related signals, as shown in Fig. 5. Figures

274 6 and 7 further illustrated the influence mechanism of Atlantic SSTA pattern onto DUCMASS. Figure 6

showed that the effect of North and South Atlantic SSTA (NorAtl/SouAtl) with ENSO signal removed

on the geopotential height (GP) at 850hPa/300hPa exhibited significant difference during P1, while they

were close (all are not significant) in P2. Similarly, significant difference was also seen in the effect of

North and South Atlantic SSTA on the zonal/meridional wind (U/V) at 300hPa in P1, which disappeared

in P2, as shown in Fig. 7. This was consistent with the variation of Atlantic SSTA's contribution to

DUCMASS–Niño-3 relationship, i.e., during P1, the Atlantic SSTA pattern was featured with a Niña type

(Fig. 3 (a)), thus the South Atlantic presented stronger influence on the atmospheric circulation over

South Asia, which weakened the impact of ENSO on DUCMASS; while in P2, the negative North

Atlantic SSTA (Fig. 3 (b)) decreased the SSTA gradient between North and South Atlantic and offset the

effect of the Niña pattern, which weakened the response of atmospheric circulation on North and South

Atlantic SSTA gradient and strengthened the DUCMASS–Niño-3 relationship.
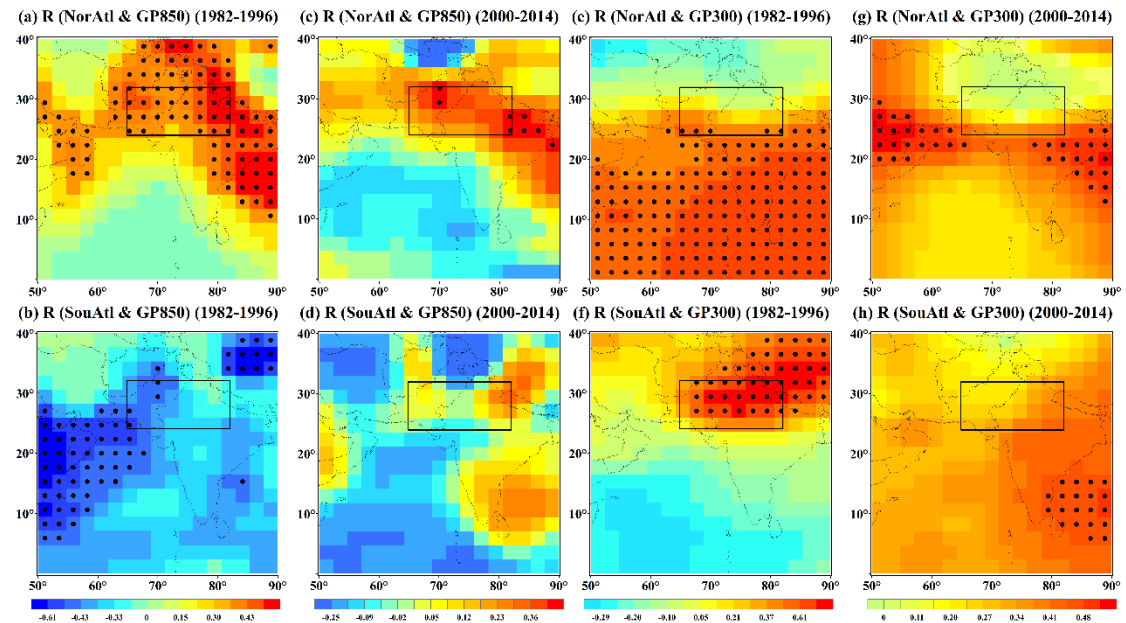
Figure 6: Correlation between spring (Mar.–May) tropical North and South Atlantic SSTA (NorAtl/SouAtl) with ENSO signal removed and geopotential height (GP) at 850hPa (a)–(d) as well as 300hPa (e)–(h) in dust season (Jun.–Jul.). (Correlations that passed the 90% confidence level were marked by black dots).
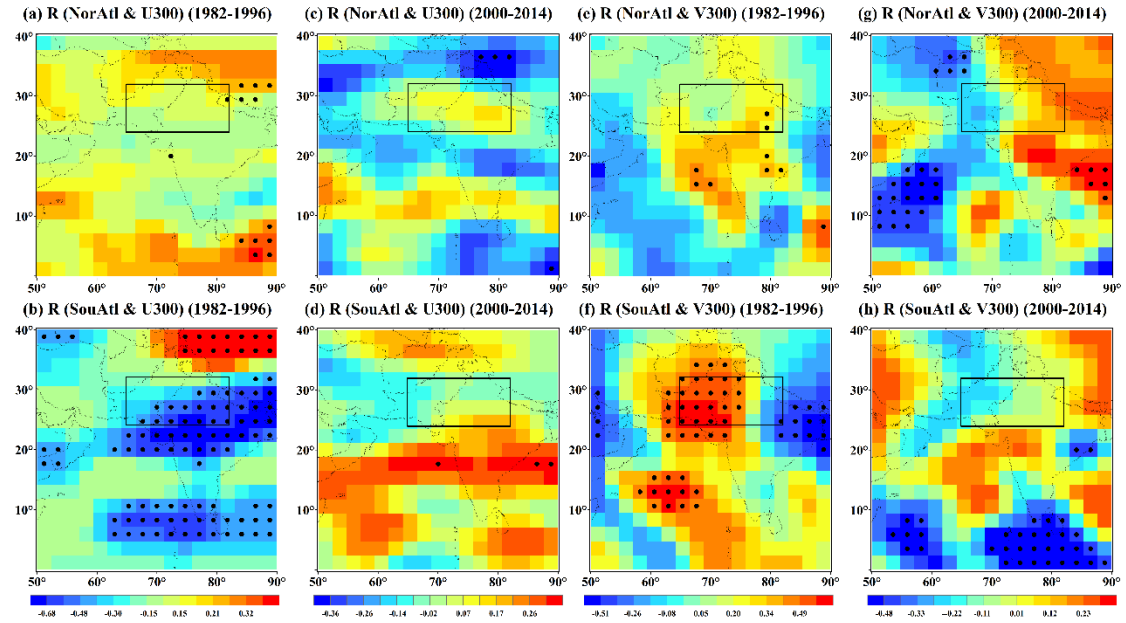
Figure 7: Correlation between spring (Mar.–May) tropical North and South Atlantic SSTA (NorAtl/SouAtl) with ENSO signal removed and zonal wind (U) (a)–(d) as well as meridional wind (V) (e)–(h) at 300hPa in dust season (Jun.–Jul.). (Correlations that passed the 90% confidence level were marked by black dots).

In order to verify the inhibitory effect of Atlantic SSTA pattern on the DUCMASS–Niño-3 relationship, we analyzed the regression of ASGI onto the local conditions that directly influenced DUCMASS, such as precipitation (PPT), soil moisture (SoilM), Normalized Difference Vegetation Index (NDVI), and air flow. Figure 8 showed that the regression coefficients between ASGI and SoilM as well as PPT and NDVI (not shown) were opposite to that between Niño-3 and SoilM during P1, while during P2, the abovementioned differences were weakened. Besides, Figure 9 demonstrated that the regression coefficients between Niño-3 and velocity potential (VP) as well as wind field at 200hpa and 850hPa were also contrary to the regression coefficients between ASGI and those factors, indicating the opposite effect of ASGI and ENSO on local wind field and convection. All of those proved the inhibitory effect of Atlantic SSTA pattern on the DUCMASS–Niño-3 relationship during P1. In addition, to further elaborate the physical mechanisms of the interaction between ENSO and dust activities, the composite differences of the abovementioned climatic variables between El Nino and La Nina years as well as that between positive ASGI (ASGI+) and negative ASGI (ASGI-) years were presented, as shown in Figs. S1–S2. Figure S1 showed that the SoilM averaged from June to July in El Niño years exhibited positive anomalies, while that in La Niña years exhibited the reversed anomalies. The differences of SoilM between ASGI+ and ASGI- during P1 were negative, which were contrary to that between El Niño and

310 La Niña conditions, while the differences during P2 reversed compared with those in P1. Simultaneously,

311 the differences of VP at 200hPa and 850hPa between ASGI+ and ASGI- also presented contrary change

312 with those between El Niño and La Niña years during P1 and P2, as shown in Fig. S2. The mechanisms

313 illustrated by the composite difference were analogous with the regression between dust activities and

314 the climatic variables, both of which clarified the effect of ASGI on the relationship between ENSO and

315 dust activities over the northwestern South Asian dust source.

316
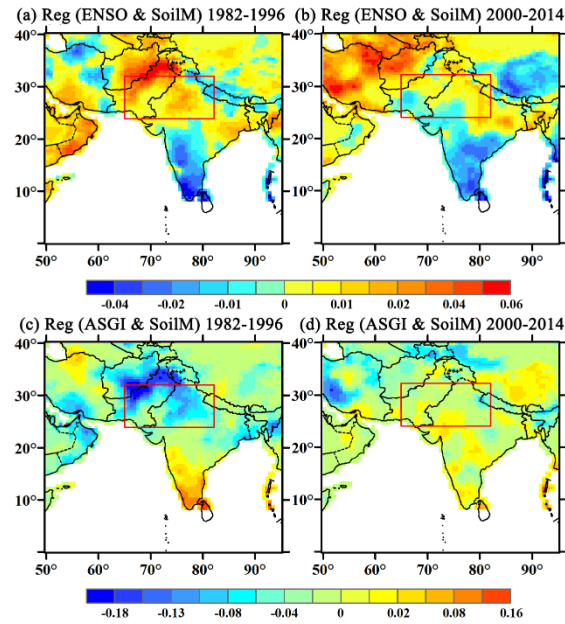
317 **Figure 8: (a)–(b) Regression of ENSO with ASGI-related signals removed onto SoilM in dust season (Jun.–**

318 **Jul.); (c)–(d) Regression of ASGI with ENSO-related signals removed onto SoilM in dust season (Jun.–Jul.).**

319
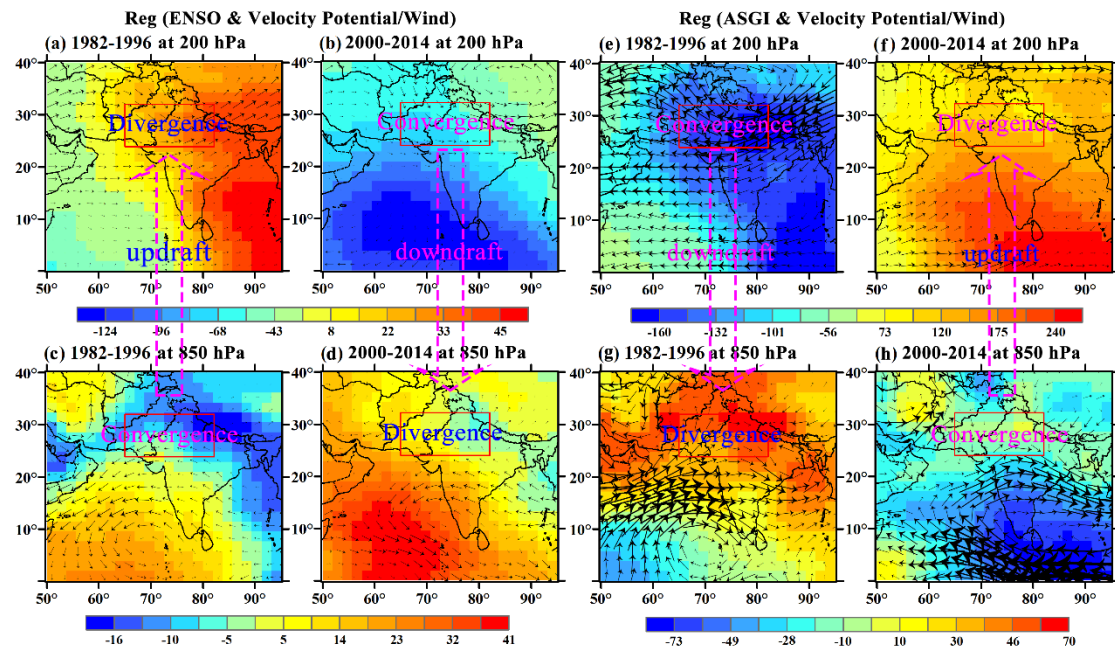
320 **Figure 9: (a)–(d) Regression of ENSO with ASGI-related signals removed onto velocity potential (VP) and**

 wind at 200hPa and 850hPa in dust season (Jun.–Jul.); (e)–(h) Regression of ASGI with ENSO-related signals

 removed onto velocity potential and wind at 200hPa and 850hPa in dust season (Jun.–Jul.).

323 **3.2.2 Tropical Indian ocean SSTA pattern**

324   This study explored the effect of Indian ocean SSTA pattern on the DUCMASS–Niño-3 relationship.

325 The covariability between the western Pacific and Indian Ocean has been widely recognized by previous

326 studies (Kug et al., 2005; Wang et al., 2003; Watanabe and Jin, 2002). ENSO can affect the Indian Ocean

327 SST in the form of Walker circulation and the Indian Ocean variability can also modulate the ENSO

328 variability (Wu and Kirtman, 2004; Yu et al., 2002; Kug et al., 2005). It is known that ENSO mainly

329 influences the monsoon rainfall of South Asia through changing the SST of Indian ocean (Krishnamurthy

330 and Kirtman, 2003; Srivastava et al., 2019). Du et al. (2009) indicated that the North Indian Ocean

331 warming displayed two peaks in Nov.–Dec.(-1) and Jun.–Aug.(0), with the second peak larger in

332 magnitude. Cherchi and Navarra (2013) also pointed out that the connection between ISM and Indian

333 ocean SST pattern was mostly confined in summer and autumn. Besides, compared to Atlantic, the Indian

334 ocean is closer to the South Asian dust source, thus it takes less time to transmit the signal (partially

335 through wave train propagation) from the Indian ocean to the dust source than that from the Atlantic.

336 Given all of that, the Indian ocean SST used in this study was the summer average that was concurrent

337 with the dust season (Jun.–Jul.).

338   The relationship between DUCMASS and Niño-3 with Indian ocean SST signal removed also

339 experienced decadal variation. Figure 10 (a) showed that the correlation between Niño-3 and DUCMASS

340 was obviously reduced when the tropical western Indian ocean SSTA (TWISST) was removed from

341 Niño-3. As illustrated by Fig. 10 (b), during P1, TWISST weakened this correlation while no significant

342 contribution was observed during P2. Thus, it is hypothesized that TWISST weakened the impact of

343 ENSO on DUCMASS during P1. However, when the IOD (rather than TWISST) was considered, the

344 correlation between Niño-3 and DUCMASS kept the same when IOD was removed from Niño-3,

345 indicating that IOD exhibited no significant impact on the correlation between Niño-3 and DUCMASS.

346 Clark et al. (2000) showed that the SST in the central Indian Ocean exhibited stronger correlation with

347 the Indian precipitation than that in the Arabian Sea and northwest of Australia. Cherchi and Navarra

348 (2013) also pointed out that when the eastern and western poles of the IOD were considered separately,

349 the western side exhibited the largest correlation. Thus, the TWISST was considered when exploring the

350 effect of Indian ocean SSTA pattern on the DUCMASS–Niño-3 relationship.

351
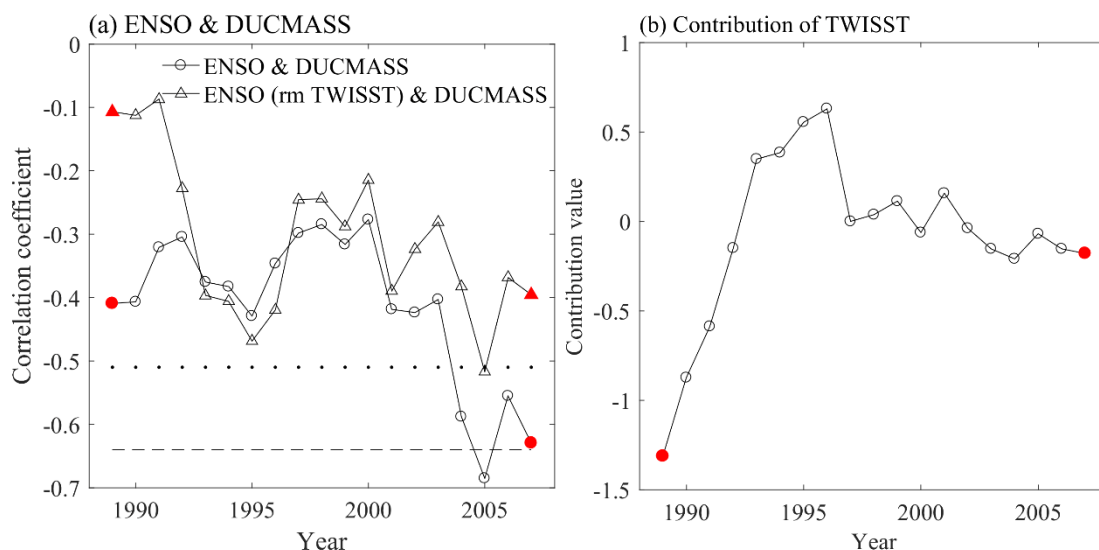
352 **Figure 10: (a) The 15-year sliding correlation between DUCMASS and Niño-3 with and without TWISST-**

353 **related signals removed; (b) Sliding contribution of TWISST to DUCMASS–Niño-3 relationship. The two red**

354 **filled markers represented the 15-year window spanning from 1982 to 1996 and 2000 to 2014, respectively.**

355 **The x-axis denotes the middle year of the period under analysis.**

356   The spatial coupling mode between DUCMASS and tropical Indian ocean SSTA showed that the

357 cold tropical western Indian ocean and warm tropical eastern Indian ocean were coupled with higher

358 DUCMASS over the northern and northwestern India. This pattern was not impacted by ENSO since the

359 MCA results with ENSO-related signals removed were similar with that including the ENSO-related

360 signals, as shown in Fig. 11. Figures 12–14 further illustrated the influence mechanism of Indian ocean

361 SSTA pattern onto DUCMASS. Figure 12 showed that during P1, the regression coefficients between

362 ENSO and PPT were opposite to the that between TWISST and PPT, while during P2, the regression

363 coefficient between ENSO and DUCMASS as well as that between TWISST and DUCMASS were all

364 positive. The similar changes were also seen when the effects of ENSO/TWISST on SoilM (Fig. 13), VP

365 and wind field (Fig. 14) were considered. These illustrated the opposite effect of TWISST and ENSO on

366 the key factors that influence the dust concentration, i.e., the local wind field and surface conditions. The

367 above results further verified the inhibitory effect of Indian ocean SST pattern on the DUCMASS–Niño-

368 3 relationship during P1, as well as the promotional effect during P2. In addition, to further elaborate the

369 physical mechanisms of the interaction between ENSO and dust activities that was impacted by tropical

370 western Indian ocean, the composite differences of the abovementioned climatic variables between El

Nino and La Nina years as well as that between positive TWITSST (TWITSST+) and negative TWITSST (TWITSST-) years were presented, as shown in Figs. S3-S5. Figures S3-S4 showed that the PPT and SoilM averaged from June to July in El Niño years exhibited positive anomalies, while that in La Niña years exhibited the reversed anomalies. The differences of PPT and SoilM between TWITSST+ and TWITSST- during P1 were negative, which were consistent with that between El Niño and La Niña conditions, while the differences during P2 were contrary to those during P1. Simultaneously, the differences of VP at 200hPa between TWITSST+ and TWITSST- also presented contrary change with those between El Niño and La Niña years during P1 and P2, as shown in Fig. S5. The mechanisms illustrated by the composite difference were analogous with the regression between dust activities and the climatic variables, both of which clarified the effect of TWITSST on the relationship between ENSO and dust activities over the northwestern South Asian dust source.
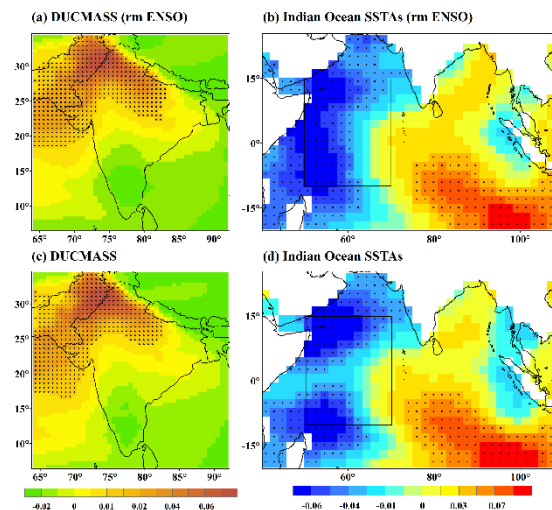
Figure 11: Spatial correlation between summer (Jun.–Jul.) tropical Indian ocean SSTA (TWISSTA) and DUCMASS of the first mode of the MCA analysis in 1982–2014. The first MCA mode of (a) the DUCMASS, and (b) the summer (Jun.-Jul.) tropical Indian ocean SSTA with ENSO-related signals removed. (c)–(d) As in (a)–(b), but for the original series including the ENSO signal. The black dots represent significance at ≥90 % confidence level.

(a) Reg (ENSO & PPT) 1982-1996 (b) Reg (ENSO & PPT) 2000-2014

388
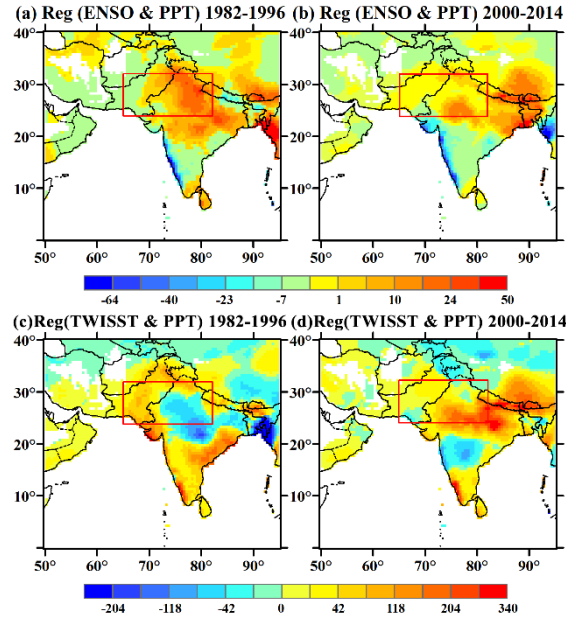
389   **Figure 12: (a)–(b) Regression of ENSO with TWISST-related signals removed onto PPT in dust season (Jun.–**

390   **Jul.); (c)–(d) Regression of TWISST with ENSO-related signals removed onto PPT in dust season (Jun.–Jul.).**

391

392   **Figure 13: (a)–(b) Regression of ENSO with TWISST-related signals removed onto SoilM in dust season**

393   **(Jun.–Jul.); (c)–(d) Regression of TWISST with ENSO-related signals removed onto SoilM in dust season**

394   **(Jun.–Jul.).**

Figure 14: (a)–(b) Regression of ENSO with TWISST-related signals removed onto velocity potential at 850hPa (VP850) and wind in dust season (Jun.–Jul.); (c)–(d) Regression of TWISST with ENSO-related signals removed onto velocity potential at 850hPa (VP850) and wind in dust season (Jun.–Jul.).

3.2.3 Pacific Decadal Oscillation

It is suggested that the PDO can influence the interannual variability of ISMR by enhancing the ENSO–ISMR relationship when ENSO and PDO were in-phase, while weakening the relationship when they were out of phase (Dong et al., 2018; Krishnamurthy and Krishnamurthy, 2014). However, it is unclear whether PDO is responsible for the shift of the DUCMASS–Niño-3 relationship. Table 2 listed the years with different phases of ENSO and PDO as well as years when ENSO and PDO are in (out of) phase separately. The correlation coefficient between ENSO and DUCMASS and significance level were also given. It demonstrated that the PDO significantly strengthened the correlation between ENSO and DUCMASS as the coefficient turned from –0.39 (P>0.1) when PDO and ENSO were out of phase to –0.69 (P<0.01) when they were in phase.

Table 2: List of individual and combined wintertime ENSO–PDO years during 1982–2014.

Events	Phase	
	Positive	Negative
ENSO	1983, 1987, 1988, 1991, 1993–1995, 1998, 2003, 2005, 2007, 2010, 2015,	1982, 1984–1986, 1989, 1996, 1997, 1999–2001, 2006, 2008, 2009, 2011,

	2016, 2019	2012, 2014
PDO	1981–1988, 1996–1998, 2001, 2003–2006, 2010, 2014–2019	1989, 1991, 1995, 1999, 2000, 2002, 2008, 2009, 2011, 2012
ENSO×PDO	1983, 1987–1989, 1998–2000, 2003, 2005, 2008–2012	1982, 1984–1986, 1991, 1995–1997, 2001, 2006, 2014
R (Niño-3 & DUCMASS)	–0.69 (P<0.01)	–0.39 (P>0.1)

410   Table 2 revealed that P2 includes most of years (8 out of 14) when ENSO and PDO were in-phase,

411   i.e., 2000, 2003, 2005, and 2008–2012, while most of the out-of-phase years (8 out of 11) appeared in

412   P1, i.e., 1982, 1984–1986, 1991, 1995, 1996, and 1997. Simultaneously, the winter Niño-3 exhibited

413   lower correlation with DUCMASS in P1 when most of ENSO years were accompanied with anti-phase

414   PDO. In addition, the quantitative contribution of PDO shown in Fig. 15 further confirmed that the PDO

415   strengthened the impact of ENSO on DUCMASS in P2 while the contribution was close to 0.0 in P1. All

416   those demonstrated that the phase shift of PDO plays an important role in modulating the revolution of

417   DUCMASS–Niño-3 relationship.
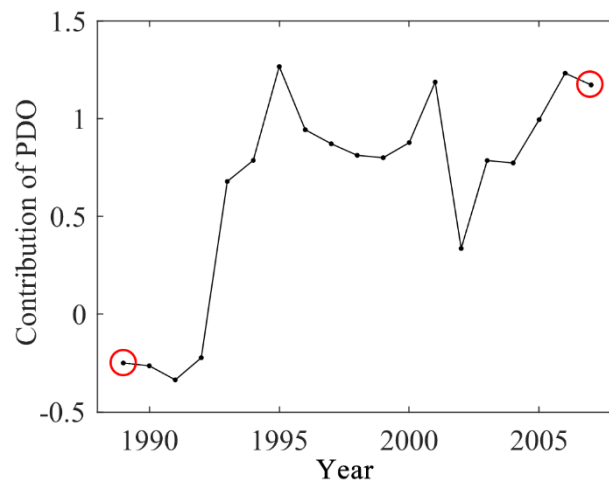
418
419   **Figure 15: Sliding contribution of PDO to DUCMASS–Niño-3 relationship. The two circles represented the**

420   **15-year window spanning from 1982 to 1996 and 2000 to 2014, respectively.**

421   Figure 16 revealed the influence mechanism of PDO onto DUCMASS. During P1, the 200hPa

422   velocity potential in the positive PDO years exhibited a decrease (convergence) over the eastern tropical

423   Pacific and an increase (divergence) over the tropical Indian Ocean and Indian subcontinent (Fig. 16 (a)).

424   The upper-level divergence over India and the adjacent seas corresponded to the anomalous ascending

425   motion, which promoted ISMR and consequently suppressed the dust storms over South Asia.

426   Meanwhile, an anomalous cyclone developed to the north of India due to the enhanced convection. The

427   westerlies on the southern flank of the cyclonic anomaly transported wet air from the Arabian Sea to the

428   northwest of India (Huang et al., 2020), which further inhibited dust emissions. While in the negative

429   PDO years during P2, the 200hPa velocity potential exhibited a decrease (convergence) over India,

430   corresponding to an anomalous descending motion, as shown in Fig. 16 (b). This descending flow

431   suppressed the Indian monsoon convection and rainfall, which consequently enhanced dust emissions.

432   Similarly, an anomalous cyclone developed over the south of India. The easterlies on the northern flank

433   of the cyclonic anomaly advected relatively drier air from the Eurasian continent to the northern India

434   (Parker et al., 2016), which favored dust emissions. The difference of flow movements and their effects

435   on dust activities between positive and negative PDO years was consistent with that between El Niño

436   and La Niña years, which further proved that PDO could significantly strengthen the effect of ENSO on

437   DUCMASS when it was in phase with ENSO.

(a) Reg of VP & UV at 200hPa onto PDO in 1982-1996
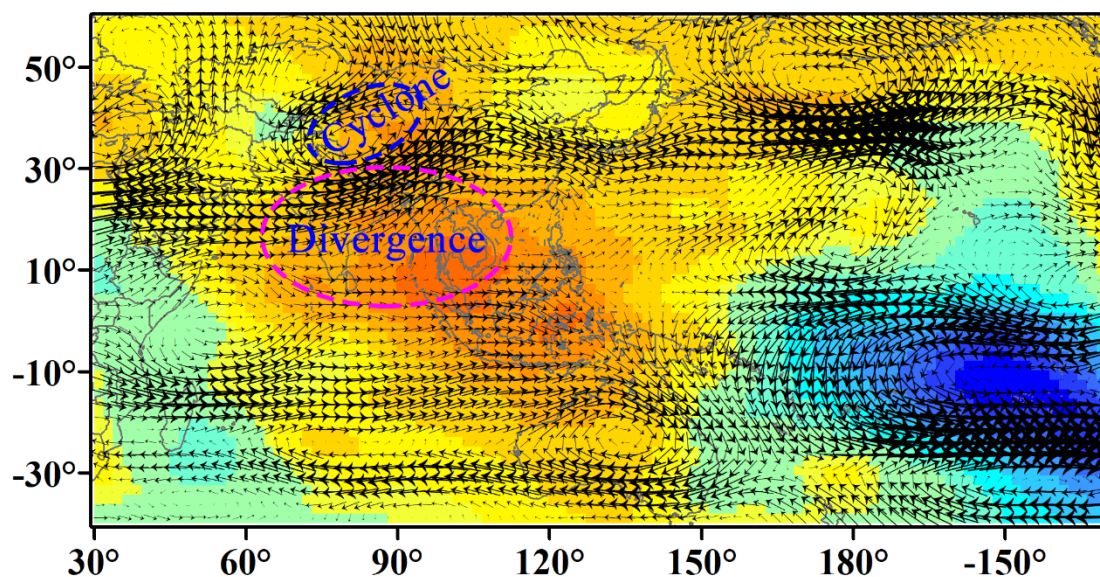
(b) Reg of VP & UV at 200hPa onto PDO in 2000-2014
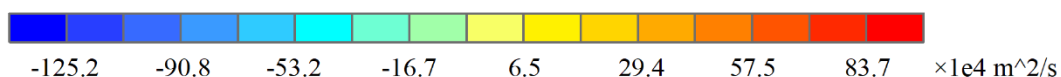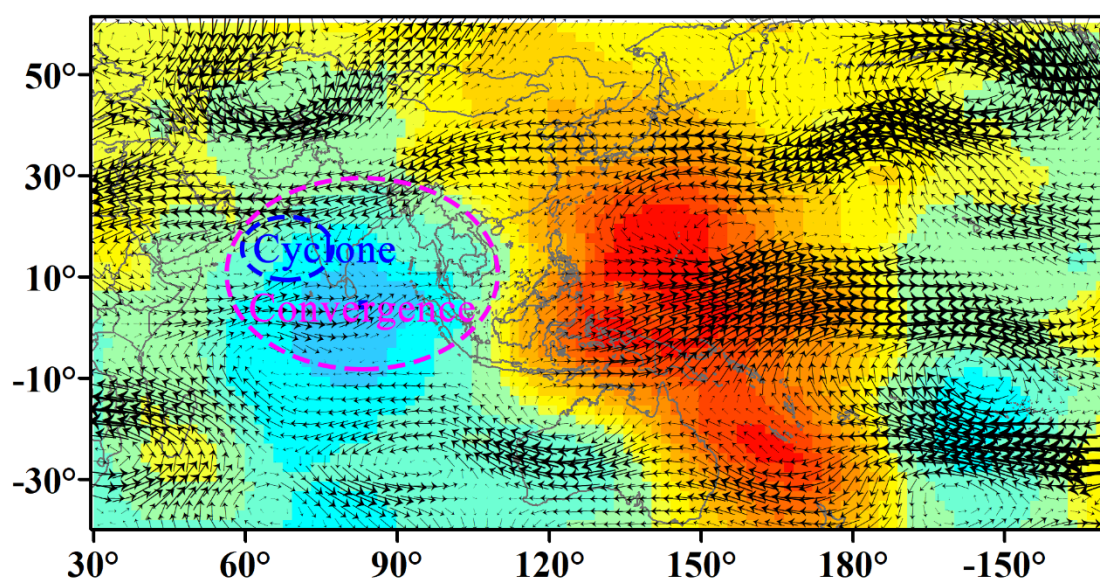
Figure 16: (a) Regression of summer (Jun.–Jul.) velocity potential at 200hPa onto previous winter PDO (averaged from Nov. to Jan.) overlaid with the average of summer wind in positive PDO years during 1982–1996; (b) Regression of summer velocity potential at 200hPa onto previous winter PDO overlaid with the average of summer wind in negative PDO years during 2000–2014.

4 Discussion

4.1 Response of Atlantic SSTA pattern to CT/EM ENSO

It was reported that the interdecadal shift of tropical Atlantic SSTA pattern was a response to the

multi-year ENSO events (Tokinaga et al., 2019). The multi-year ENSO event, namely continuing ENSO (CT ENSO), was a situation where the summer ENSO SSTA continued from the preceding year. Another type of ENSO, which was called as emerging ENSO (EM ENSO), was characterized as late Atlantic SSTA response that started from June. The CT ENSO primarily dominated during P1, while P2 was dominated by EM ENSO (Yang and Huang, 2021). The impact of the two types of ENSO on the shift of the DUCMASS–Niño-3 relationship were examined. Table 3 showed that ASGI was significantly correlated with Niño-3 in the CT ENSO years, which was not observed in the EM ENSO years. Simultaneously, DUCMASS was significantly related to Niño-3 only in the EM ENSO years. The composite correlation difference between CT and EM ENSOs was consistent with that between the period of P1 and P2, indicating that the shift of Atlantic SSTA pattern, which was prominently modulated by the type of ENSO, plays an important role in modulating the DUCMASS–Niño-3 relationship.

Table 3: Correlation between ASGI and Niño-3 as well as DUCMASS in two different phases (* and *** indicate the correlations that are significant on a 0.1 and 0.01 level, respectively).

R	CT ENSO	EM ENSO	P1	P2
ASGI & Niño-3	0.78 (***)	0.19	0.73 (***)	0.46 (*)
DUCMASS & Niño-3	-0.60 (*)	-0.75 (***)	-0.51 (*)	-0.67 (***)

4.2 Response of Indian ocean SSTA pattern to CT/EM ENSO

As discussed in Sect. 3.2.2, ENSO can affect the Indian Ocean SST and the Indian Ocean variability can also modulate the ENSO variability (Wu and Kirtman, 2004; Yu et al., 2002; Kug et al., 2005). It is known that during CT ENSO years, the ENSO event in summer primarily starts from the preceding winter, while in EM ENSO years, the ENSO event mainly emerges in late spring (Yang and Huang, 2021). Correspondingly, the associated Indian Ocean SST oscillation also varies in these two different ENSO years. In order to explore whether the different types of ENSO impacted the DUCMASS over the northwestern South Asia through adjusting the duration of the temperature anomaly, we compared the SST and the variance of the monthly SSTA from (–1) Sep. to (0) May over the tropical western Indian ocean (TWISSTA).

Figure 17 (a) showed that the variances in the EM La Niña years were generally larger than that in

471 the CT La Niña years, while the variances in the EM El Niño years were generally smaller than that in

472 the CT El Niño years. Concurrently, the difference of DUCMASS in El Niño and La Niña years was

473 obvious in the EM ENSO period with higher values appeared in La Niña years (Fig. 17 (b)). However,

474 in the CT ENSO period, no significant difference was observed between El Niño and La Niña years.

475 Therefore, it is hypothesized that the EM ENSO conditions, which was associated with higher TWISST

476 variance, were more favorable to trigger the variation of DUCMASS. Yang and Huang (2021) reported

477 that P1 was primarily dominated by CT ENSOs while EM ENSOs primarily controlled during P2.

478 Combined with abovementioned hypothesis, the correlation between DUCMASS and Niño-3 should be

479 higher in P2, which was consistent with the interdecadal change of this relationship. Figure 17 (c) further

480 revealed the influence mechanism of TWISSTA onto DUCMASS. It showed that compared to CT ENSO

481 type, the difference of PPT between El Niño and La Niña years was more significant in the EM ENSO

482 years, in addition, the PPT in La Niña years (with high TWISSTA variance) was lower than that in El

483 Niño years (with low TWISSTA variance), which was contrary to the difference of DUCMASS between

484 those two types of ENSO years. While when other atmospheric factors were considered, such as land

485 cover and winds at multi-layers, no similar change was observed. This indicated that the Indian Ocean

486 SSTA, which was also remarkably modulated by the type of ENSO, impacted DUCMASS by adjusting

487 the PPT and further influenced the relationship between ENSO and DUCMASS.

488
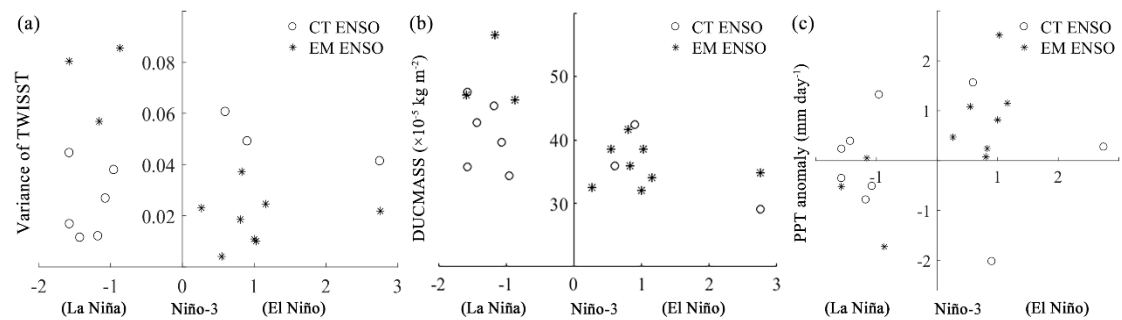
489 **Figure 17: Scatter diagram between (a) variance of the monthly TWISSTA from (−1) Sep. to (0) May, (b)**

490 **DUCMASS, and (c) PPT anomaly and Niño-3 index separately for continuing (CT) and emerging (EM) ENSO.**

491 **4.3 Uncertainty in analyzing the contribution of the influence factors**

492   The contributions of those abovementioned factors to the interdecadal shift of ENSO-DUCMASS

493 relationship were analyzed based on the linear regression model. However, the linear regression model

494 would definitely bring uncertainty to the results (Guo et al., 2017) and may not be sufficient to verify the

495 cause and effect. Thus, the numerical models are suggested for future research to quantify the

496 contribution of those factors to the shift of ENSO–DUCMASS relationship. However, before such

497 quantitative study the regression analysis is indispensable to identify the possible driving factors. In this

498 context, it is undeniable that this study provides new sights to the dust storm-related numerical simulation

499 by taking account of the teleconnections and their influence mechanisms.

500 In addition, while analyzing the effects of different types of ENSO event, we compared the variance

501 of TWISST and DUCMASS under the two types of ENSO periods, as shown in Fig. 17. It showed that

502 only eight EM ENSO years were identified and the number of PDO years that were in or out of phase

503 with ENSO were also insufficient. The statistical results acquired from the insufficient number of

504 samples could also be explained by the random events (Pallikari, 2004). In order to verify this conclusion,

505 we calculated the interannual correlation between the variance of TWISST and DUCMASS from 1982

506 to 2014. Even so, the significant interannual correlation does not guarantee the significant link between

507 different types of ENSO. Therefore, longer time series with valid samples (i.e., CT/EM ENSO and PDO

508 years) are needed to further validate the influence of ENSO types on the ENSO–DUCMASS relationship

509 in the future. Alternatively, using numerical model to simulate the teleconnection pattern of ENSO over

510 South Asia under different types of ENSO is also favorable.

511 Except for the large-scale atmospheric circulation, the anthropogenic land-use management could

512 also play an important role in the interdecadal variability of ENSO–DUCMASS relationship (Kumar et

513 al., 1999), which should be considered in the future researches.

514 The dust activities analyzed in this study were from the dust season, i.e., Jun.–Jul., which were part

515 of monsoon season (Jun.–Sep.) (Babu et al., 2013), however, the dust activities during pre-monsoon

516 season (Mar.–May or Apr.–May) were also a hot topic (Babu et al., 2013; Lakshmi et al., 2017, 2019).

517 Therefore, we analyzed the interdecadal change of the ENSO impact on DUCMASS during dust season

518 (Jun.–Jul.) and pre-monsoon (Mar.–May or Apr.–May) separately, to find that the significant interdecadal

519 change occurred only when the DUCMASS during dust season was considered. As for that during pre-

520 monsoon season, there should be some other factors that influenced its interdecadal change, which will

521 be discussed in the future study.

522 **4.4 Precision validation of MERRA-2 dust concentration dataset**

523   It is known that the nonspherical aerosol optical depth retrieved from satellite, concentration of

524   PM2.5/PM10 and coarse mode aerosol optical depth acquired from observation stations represent

525   extinction characteristics of dust aerosols in the whole atmospheric column, thus they can be used to

526   validate the dust column concentration datasets but not appropriate for the validation of dust emission,

527   which reflect the dust loading lifted from ground. The dust dataset used in this study was the dust column

528   concentration "Dust Column Mass Density-PM$_{2.5}$", thus the PM$_{2.5}$, coarse mode aerosol optical depth

529   acquired from AERONET (AERONET/DOD), and nonspherical aerosol optical depth retrieved from

530   MISR (MISR/DOD) was utilized to validate the precision of DUCMASS dataset. The time coverage and

531   continuity of satellite and observation-based products lagged behind the MERRA-2 datasets, thus only

532   several stations over the dust belt with relatively longer time series were chosen. They were Kanpur (26.5°

533   N, 80.2° E. Time span: 2001–2021), Sede Boker (30.9° N, 34.8° E. Time span: 2007–2019), and

534   Tamanrasset INM (22.8° N, 5.5° E. Time span: 2007–2019). The MISR/DOD, PM2.5, and dust variables

535   from MERRA-2 were the regional average within 1° of the corresponding station. No dust emission was

536   observed over the Kanpur and Tamanrasset INM station. Besides, the datasets over the study area

537   (represented by Thar desert in Fig. 18 (a)) were also accounted and the AERONET/DOD was obtained

538   from the nearest Kanpur station. For the study area, PM$_{2.5}$ was chosen as the reference dataset (A) because

539   the study area was not overlapped with the Kanpur station, while AERONET/DOD was chosen as the

540   reference data for other stations.
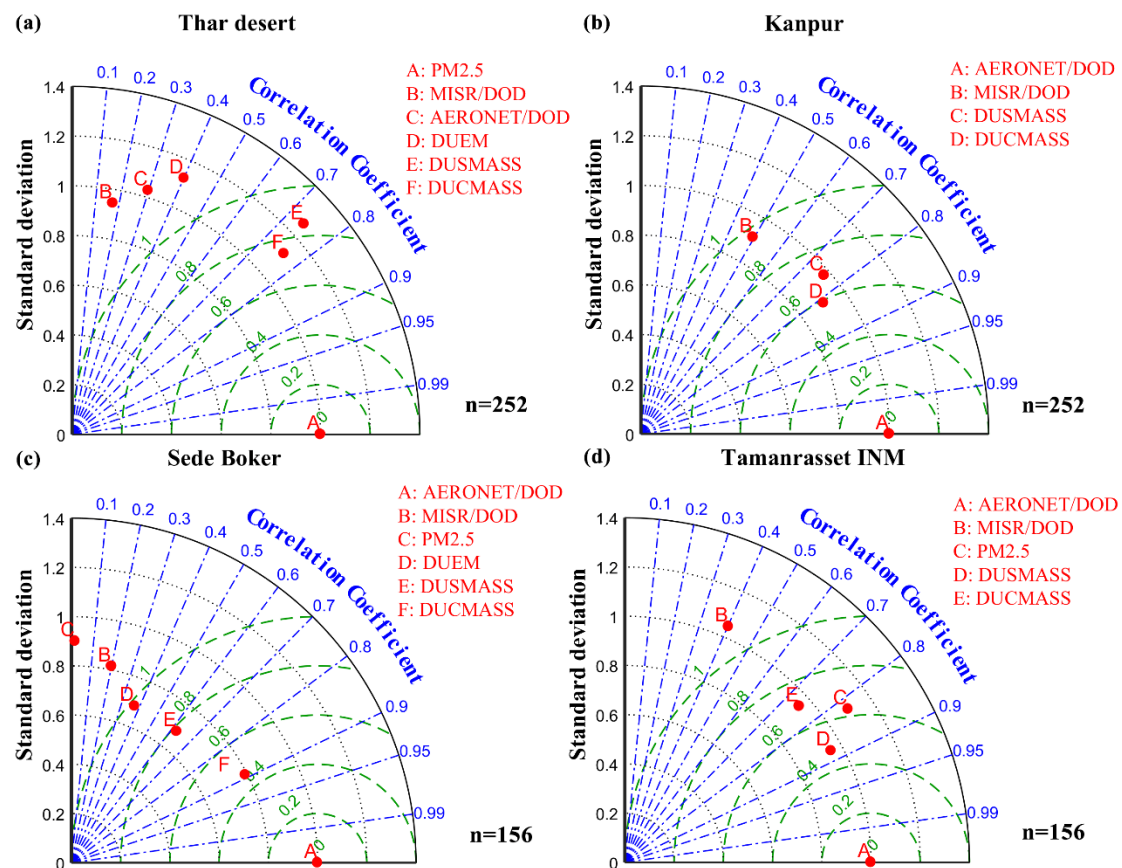
Figure 18: Normalized Taylor diagrams showing (a) difference between dust variables acquired from MISR, AERONET, MERRA2 datasets and that acquired from PM2.5 dataset, and (b–d) difference between dust variables from MISR, PM2.5, MERRA2 datasets and that acquired from AERONET dataset. The normalized standard deviation is on the radial axis (black contours); correlation coefficient is on the angular axis (blue contours); and green dashed lines indicate centered RMSE. N indicates the sample size.

Figure 18 (a) compared the precision of MISR/DOD, AERONET/DOD, dust emission (DUEM), surface dust mass concentration (DUSMASS), and DUCMASS with that of PM$_{2.5}$, it showed that no significant correlation was observed between AERONET/DOD and PM$_{2.5}$ because this study area did not coincide with the Kanpur station. However, the correlations between PM$_{2.5}$ and DUSMASS as well as DUCMASS were significant (R>0.7, RMSE<0.9) and stronger than that between PM$_{2.5}$ and DUEM. Figure 18 (b) showed the precision of MISR/DOD, DUSMASS, and DUCMASS compared with AERONET/DOD over the Kanpur station. The results indicated that both DUSMASS and DUCMASS were significantly correlated with AERONET/DOD (R>0.7, RMSE<0.8). In addition, the comparison results over the other two stations also indicated that DUSMASS and DUCMASS were significantly correlated with AERONET/DOD, while the relationship between DUEM and AERONET/DOD was weak, as shown in Figs. 18 (c)–(d). The above results demonstrated that the DUCMASS from MERRA-2 was strongly consistent with MISR/DOD, AERONET/DOD, and PM$_{2.5}$, indicating that the DUCMASS

559   datasets used in this study were relatively reliable for researches about dust.

560   **5 Conclusions**

561   In the study, we revealed the interdecadal change of the ENSO impact on DUCMASS over the

562   northwestern South Asia from 1982 to 2014, and further investigated the factors contributing to the shifts

563   of the responses of DUCMASS to the wintertime ENSO. It was found that the ENSO–DUCMASS

564   relationship shifted from weak negative relation during 1982–1996 to significant negative correlation

565   during 2000–2014. The change of Atlantic and Indian ocean SSTA pattern weakened the impact of

566   wintertime ENSO on dust activities over the northwestern South Asia during 1982–1996, while PDO

567   tended to strengthen ENSO's effect on dust activities when it was in phase with ENSO. Both the Atlantic

568   and Indian Ocean SSTA patterns were modulated by the duration of ENSO events (i.e., continuing and

569   emerging ENSO). The current results are based solely on the linear regression, and further studies

570   integrating numerical models and longer time series are needed to validate the results. Nevertheless, this

571   study indeed found multiple large-scale factors that could impact the interdecadal interaction between

572   ENSO and dust activities over the northwestern South Asia. Given that it is possible to forecast the

573   change of some large-scale atmospheric circulation patterns, the results of this study could provide new

574   insight to the prediction of dust storm trend in the near future based on the variability of ENSO–

575   DUCMASS relationship.

576   **Data availability**

577   The data can be downloaded for free from the corresponding website which were listed in the text.

578   **Author contribution**

579   L.S. designed the study, performed the analysis with feedback from J.Z. and F.Y., and wrote the

580   paper that was reviewed by J.Z., F.Y., D.Z., J.W., X.M., and Y.L.. All the authors discussed the results.

581   **Competing interests**

582   The authors declare that they have no conflict of interest.

Acknowledgments

The authors would like to thank the Modern-Era Retrospective Analysis for Research and Applications, version 2 (MERRA-2) for providing the surface dust mass concentration, wind speed and planetary boundary layer height, the National Oceanic and Atmospheric Administration (NOAA) for providing the SST, the Hadley Centre Climate Research Unit for the land-surface temperature and precipitation, the National Aeronautics and Space Administration (NASA) for the NDVI, and the Climate Predict Center of National Oceanic and Atmospheric Administration (NOAA/CPC) for the large-scale climate indices.

This work was supported by the Strategic Priority Research Program of the Chinese Academy of Sciences-A (No. XDA19030402) and the National Natural Science Foundation of China (No. 42071425).

References

Abish, B. and Mohanakumar, K.: Absorbing aerosol variability over the Indian subcontinent and its increasing dependence on ENSO, Glob. Planet. Change, 106, 13–19, https://doi.org/10.1016/j.gloplacha.2013.02.007, 2013.

Ashok, K., Behera, S. K., Rao, S. A., Weng, H., and Yamagata, T.: El Nino Modoki and its possible teleconnection, J. Geophys. Res., 112, C11007, 2007.

Augustyn, A., Zeidan, A., Zelazko, A., Eldridge, A., McKenna, A., Tikkanen, A., Gadzikowski, A., Schreiber, B. A., Duignan, B., Mahajan, D., Promeet, D., Goldstein, E., and Rodriguez, E.: Thar Desert, Encycl. Br., 2019.

Avila, A.: The chemical composition of dust transported in red rains—its contribution to the biogeochemical cycle of a holm oak forest in Catalonia (Spain), Atmos. Environ., 32, 179–191, 1998.

Babu, S. S., Manoj, M. R., Moorthy, K. K., Gogoi, M. M., Nair, V. S., Kompalli, S. K., Satheesh, S. K., Niranjan, K., Ramagopal, K., Bhuyan, P. K., and Singh, D.: Trends in aerosol optical depth over Indian region: Potential causes and impact indicators, J. Geophys. Res. Atmos., 118, 11,794-11,806, https://doi.org/10.1002/2013JD020507, 2013.

Banerjee, P. and Kumar, S. P.: ENSO modulation of interannual variability of dust aerosols over the northwest Indian Ocean, J. Clim., 29, 1391–1415, https://doi.org/10.1175/JCLI-D-15-0039.1, 2016.

610   Banerjee, P., Satheesh, S. K., Moorthy, K. K., Nanjundiah, R. S., and Nair, V. S.: Long-range transport

611   of mineral dust to the northeast Indian Ocean: Regional versus remote sources and the implications,

612   J. Clim., 32, 1525–1549, https://doi.org/10.1175/JCLI-D-18-0403.1, 2019.

613   Behrooz, R. D., Esmaili-Sari, A., Bahramifar, N., and Kaskaoutis, D. G.: Analysis of the TSP, PM10

614   concentrations and water-soluble ionic species in airborne samples over Sistan, Iran during the

615   summer dusty period, Atmos. Pollut. Res., 8, 403–417, 2017.

616   Bollasina, M. A., Ming, Y., and Ramaswamy, V.: Anthropogenic aerosols and the weakening of the

617   south asian summer monsoon, Science (80-.)., 334, 502–505,

618   https://doi.org/10.1126/science.1204994, 2011.

619   Bozlaker, A., Prospero, J. M., Fraser, M. P., and Chellam, S.: Quantifying the contribution of long-range

620   saharan dust transport on particulate matter concentrations in Houston, Texas, using detailed

621   elemental analysis, Environ. Sci. Technol., 47, 10179–10187, https://doi.org/10.1021/es4015663,

622   2013.

623   Buchard, V., Randles, C. A., da Silva, A. M., Darmenov, A., Colarco, P. R., Govindaraju, R., Ferrare,

624   R., Hair, J., Beyersdorf, A. J., Ziemba, L. D., and Yu, H.: The MERRA-2 aerosol reanalysis, 1980

625   onward. Part II: Evaluation and case studies, J. Clim., 30, 6851–6872, https://doi.org/10.1175/JCLI-

626   D-16-0613.1, 2017.

627   Cai, W., Borlace, S., Lengaigne, M., Van Rensch, P., Collins, M., Vecchi, G., Timmermann, A., Santoso,

628   A., Mcphaden, M. J., Wu, L., England, M. H., Wang, G., Guilyardi, E., and Jin, F. F.: Increasing

629   frequency of extreme El Niño events due to greenhouse warming, Nat. Clim. Chang., 4, 111–116,

630   https://doi.org/10.1038/nclimate2100, 2014.

631   Chauhan, S. S.: Desertification control and management of land degradation in the Thar desert of India,

632   Environmentalist, 23, 219–227, https://doi.org/10.1023/B:ENVR.0000017366.67642.79, 2003.

633   Chen, Y.-S., Sheen, P.-C., Chen, E.-R., Liu, Y.-K., Wu, T.-N., and Yang, C.-Y.: Effects of Asian dust

634   storm events on daily mortality in Taipei, Taiwan., Environ. Res., 95, 151–155,

635   https://doi.org/10.1016/j.envres.2003.08.008, 2004.

636   Cherchi, A. and Navarra, A.: Influence of ENSO and of the Indian Ocean Dipole on the Indian summer

637   monsoon variability, Clim. Dyn., 41, 81–103, https://doi.org/10.1007/s00382-012-1602-y, 2013.

638   Clark, C. O., Cole, J. E., and Webster, P. J.: Indian Ocean SST and Indian summer rainfall: Predictive

639   relationships and their decadal variability, J. Clim., 13, 2503–2519, https://doi.org/10.1175/1520-

640   0442(2000)013<2503:IOSAIS>2.0.CO;2, 2000.

641   Dong, B., Dai, A., Vuille, M., and Timm, O. E.: Asymmetric modulation of ENSO teleconnections by

642   the interdecadal Pacific oscillation, J. Clim., 31, 7337–7361, https://doi.org/10.1175/JCLI-D-17-

643   0663.1, 2018.

644   Du, Y., Xie, S. P., Huang, G., and Hu, K.: Role of air-sea interaction in the long persistence of El Niño-

645   induced   north   Indian   Ocean   warming,   J.   Clim.,   22,   2023–2038,

646   https://doi.org/10.1175/2008JCLI2590.1, 2009.

647   Easterling, D. R. and Wehner, M. F.: Is the climate warming or cooling?, Geophys. Res. Lett., 36, 4–6,

648   https://doi.org/10.1029/2009GL037810, 2009.

649   Erel, Y., Dayan, U., Rabi, R., Rudich, Y., and Stein, M.: Trans boundary transport of pollutants by

650   atmospheric mineral dust, Environ. Sci. Technol., 40, 2996–3005, https://doi.org/10.1021/es051502l,

651   2006.

652   Fyfe, J. C., Merryfield, W. J., Kharin, V., Boer, G. J., Lee, W. S., and Von Salzen, K.: Skillful predictions

653   of decadal trends in global mean surface temperature, Geophys. Res. Lett., 38, 1–5,

654   https://doi.org/10.1029/2011GL049508, 2011.

655   Fyfe, J. C., Gillett, N. P., and Zwiers, F. W.: Overestimated global warming over the past 20 years, Nat.

656   Clim. Chang., 3, 767–769, https://doi.org/10.1038/nclimate1972, 2013.

657   Gelaro, R., McCarty, W., Suárez, M. J., Todling, R., Molod, A., Takacs, L., Randles, C. A., Darmenov,

658   A., Bosilovich, M. G., Reichle, R., Wargan, K., Coy, L., Cullather, R., Draper, C., Akella, S., Buchard,

659   V., Conaty, A., da Silva, A. M., Gu, W., Kim, G. K., Koster, R., Lucchesi, R., Merkova, D., Nielsen,

660   J. E., Partyka, G., Pawson, S., Putman, W., Rienecker, M., Schubert, S. D., Sienkiewicz, M., and

661   Zhao, B.: The modern-era retrospective analysis for research and applications, version 2 (MERRA-

662   2), J. Clim., 30, 5419–5454, https://doi.org/10.1175/JCLI-D-16-0758.1, 2017.

663   Graham, N. E.: Decadal-scale climate variability in the tropical and North Pacific during the 1970s and

664   1980s: observations   and   model   results,   Clim.   Dyn.,   10,   135–162,

665   https://doi.org/10.1007/BF00210626, 1994.

666   Guo, H., Wang, X., and Gao, Z.: Uncertain linear regression model and its application, J. Intell. Manuf.,

667   28, 559–564, https://doi.org/10.1007/s10845-014-1022-4, 2017.

668   Hansen, J. E., Sato, M., and Ruedy, R.: Radiative forcing and climate response, J. Geophys. Res. Atmos.,

669   102, 6831–6864, 1997.

670   He, L., Lin, A., Chen, X., Zhou, H., Zhou, Z., and He, P.: Assessment of MERRA-2 Surface PM2.5 over

671   the Yangtze River Basin: Ground-based verification, spatiotemporal distribution and meteorological

672   dependence, Remote Sens., 11, 460, https://doi.org/10.3390/rs11040460, 2019.

673   He, S. and Wang, H.: Oscillating relationship between the East Asian Winter Monsoon and ENSO, J.

674   Clim., 26, 9819–9838, https://doi.org/10.1175/JCLI-D-13-00174.1, 2013.

675   Hirahara, S., Ishii, M., and Fukuda, Y.: Centennial-scale sea surface temperature analysis and its

676   uncertainty, J. Clim., 27, 57–75, https://doi.org/10.1175/JCLI-D-12-00837.1, 2014.

677   Hu, S. and Fedorov, A. V.: The extreme El Niño of 2015–2016 and the end of global warming hiatus,

678   Geophys. Res. Lett., 44, 3816–3824, https://doi.org/10.1002/2017GL072908, 2017.

679   Huang, J., Wang, T., Wang, W., Li, Z., and Yan, H.: Climate effects of dust aerosols over East Asian

680   arid   and   semiarid   regions,   J.   Geophys.   Res.   Atmos.,   119,   11398–11416,

681   https://doi.org/10.1038/175238c0, 2014.

682   Huang, X., Zhou, T., Turner, A., Dai, A., Chen, X., Clark, R., Jiang, J., Man, W., Murphy, J., Rostron,

683   J., Wu, B., Zhang, L., Zhang, W., and Zou, L.: The recent decline and recovery of Indian summer

684   monsoon rainfall: Relative roles of external forcing and internal variability, J. Clim., 33, 5035–5060,

685   https://doi.org/10.1175/JCLI-D-19-0833.1, 2020.

686   Jin, Q. and Wang, C.: The greening of Northwest Indian subcontinent and reduction of dust abundance

687   resulting from Indian summer monsoon revival, Sci. Rep., 8, 1–9, https://doi.org/10.1038/s41598-

688   018-23055-5, 2018.

689   Jin, Q., Wei, J., Pu, B., Yang, Z. L., and Parajuli, S. P.: High Summertime Aerosol Loadings Over the

690   Arabian Sea and Their Transport Pathways, J. Geophys. Res. Atmos., 123, 10,568-10,590,

691   https://doi.org/10.1029/2018JD028588, 2018.

692   Jin, Q., Wei, J., Lau, W. K. M., Pu, B., and Wang, C.: Interactions of Asian mineral dust with Indian

693   summer   monsoon: Recent   advances   and   challenges,   Earth-Science   Rev.,   215,   103562,

694   https://doi.org/10.1016/j.earscirev.2021.103562, 2021.

695   Kaiser, J. and Granmar, M.: Mounting Evidence Indicts Fine-Particle Pollution, Science (80-.)., 307,

696   1858–1861, 2005.

697   Kinter, I. L., Miyakoda, K., and Yang, S.: Recent change in the connection from the Asian monsoon to

698   ENSO,   J.   Clim.,   15,   1203–1215,   https://doi.org/10.1175/1520-

699   0442(2002)015<1203:RCITCF>2.0.CO;2, 2002.

700   Kosaka, Y. and Xie, S. P.: Recent global-warming hiatus tied to equatorial Pacific surface cooling, Nature,

701   501, 403–407, https://doi.org/10.1038/nature12534, 2013.

702   Krishnamurthy, L. and Krishnamurthy, V.: Influence of PDO on South Asian summer monsoon and

703   monsoon-ENSO relation, Clim. Dyn., 42, 2397–2410, https://doi.org/10.1007/s00382-013-1856-z,

704   2014.

705   Krishnamurthy, V. and Kirtman, B. P.: Variability of the Indian Ocean: Relation to monsoon and ENSO,

706   Q. J. R. Meteorol. Soc., 129, 1623–1646, https://doi.org/10.1256/qj.01.166, 2003.

707   Kucharski, F., Bracco, A., Yoo, J. H., and Molteni, F.: Low-frequency variability of the Indian monsoon-

708   ENSO relationship and the tropical Atlantic: The "weakening" of the 1980s and 1990s, J. Clim., 20,

709   4255–4266, https://doi.org/10.1175/JCLI4254.1, 2007.

710   Kug, J. S., An, S. Il, Jin, F. F., and Kang, I. S.: Preconditions for El Niño and La Niña onsets and their

711   relation to the Indian Ocean, Geophys. Res. Lett., 32, 1–5, https://doi.org/10.1029/2004GL021674,

712   2005.

713   Kumar, K. K., Rajagopalan, B., and Cane, M. A.: On the weakening relationship between the indian

714   monsoon   and   ENSO,   Science   (80-.   ).,   284,   2156–2159,

715   https://doi.org/10.1126/science.284.5423.2156, 1999.

716   Lakshmi, N. B., Nair, V. S., and Suresh Babu, S.: Vertical structure of aerosols and mineral dust over

717   the Bay of Bengal from multisatellite observations, J. Geophys. Res. Atmos., 122, 12,845-12,861,

718   https://doi.org/10.1002/2017JD027643, 2017.

719   Lakshmi, N. B., Babu, S. S., and Nair, V. S.: Recent Regime Shifts in Mineral Dust Trends over South

720   Asia from Long-Term CALIPSO Observations, IEEE Trans. Geosci. Remote Sens., 57, 4485–4489,

721   https://doi.org/10.1109/TGRS.2019.2891338, 2019.

722 Lee, Y. G., Kim, J., Ho, C. H., An, S. Il, Cho, H. K., Mao, R., Tian, B., Wu, D., Lee, J. N., Kalashnikova,

723 O., Choi, Y., and Yeh, S. W.: The effects of ENSO under negative AO phase on spring dust activity

724 over northern China: An observational investigation, Int. J. Climatol., 35, 935–947,

725 https://doi.org/10.1002/joc.4028, 2015.

726 Li, T., Zhang, Y., Lu, E., and Wang, D.: Relative role of dynamic and thermodynamic processes in the

727 development of the Indian Ocean dipole: An OGCM diagnosis, Geophys. Res. Lett., 29,

728 https://doi.org/10.1029/2002GL015789, 2002.

729 Liu, J., Wu, D., Liu, G., Mao, R., Chen, S., Ji, M., Fu, P., Sun, Y., Pan, X., Jin, H., Zhou, Y., and Wang,

730 X.: Impact of Arctic amplification on declining spring dust events in East Asia, Clim. Dyn., 54, 1913–

731 1935, https://doi.org/10.1007/s00382-019-05094-4, 2020.

732 Mahowald, N., Albani, S., Kok, J. F., Engelstaeder, S., Scanza, R., Ward, D. S., and Flanner, M. G.: The

733 size distribution of desert dust aerosols and its impact on the Earth system, Aeolian Res., 15, 53–71,

734 https://doi.org/10.1016/j.aeolia.2013.09.002, 2014.

735 Mahowald, N. M., Yoshioka, M., Collins, W. D., Conley, A. J., Fillmore, D. W., and Coleman, D. B.:

736 Climate response and radiative forcing from mineral aerosols during the last glacial maximum, pre-

737 industrial, current and doubled-carbon dioxide climates, Geophys. Res. Lett., 332, 382–385, 2006.

738 Mahowald, N. M., Kloster, S., Engelstaedter, S., Moore, J. K., Mukhopadhyay, S., McConnell, J. R.,

739 Albani, S., Doney, S. C., Bhattacharya, A., Curran, M. A. J., Flanner, M. G., Hoffman, F. M.,

740 Lawrence, D. M., Lindsay, K., Mayewski, P. A., Neff, J., Rothenberg, D., Thomas, E., Thornton, P.

741 E., and Zender, C. S.: Observed 20th century desert dust variability: Impact on climateand

742 biogeochemistry, Atmos. Chem. Phys., 10, 10875–10893, https://doi.org/10.5194/acp-10-10875-

743 2010, 2010.

744 Miller, R. L. and Tegen, I.: Climate response to soil dust aerosols, J. Clim., 11, 3247–3267,

745 https://doi.org/10.1175/1520-0442(1998)011<3247:CRTSDA>2.0.CO;2, 1998.

746 Nitta, T. and Yamada, S.: Recent warming of tropical sea surface temperature and its relationship to the

747 Northern Hemisphere circulation, J. Meteorol. Soc. Japan, 67, 375–383,

748 https://doi.org/10.2151/jmsj1965.67.3_375, 1989.

749 Osborn, T. J., Jones, P. D., Lister, D. H., Morice, C. P., Simpson, I. R., Winn, J. P., Hogan, E., and Harris,

750   I. C.: Land Surface Air Temperature Variations Across the Globe Updated to 2019: The CRUTEM5

751   Data Set, J. Geophys. Res. Atmos., 126, https://doi.org/10.1029/2019JD032352, 2021.

752   Pallikari, F.: On the false hypothesis of psi-mediated shift of statistical average in tests with random

753   number generators, in: The Parapsychological Association Convention 2004, 157–171,

754   https://doi.org/10.13140/2.1.4054.5289, 2004.

755   Parker, D. J., Willetts, P., Birch, C., Turner, A. G., Marsham, J. H., Taylor, C. M., Kolusu, S., and Martin,

756   G. M.: The interaction of moist convection and mid-level dry air in the advance of the onset of the

757   Indian monsoon, Q. J. R. Meteorol. Soc., 142, 2256–2272, https://doi.org/10.1002/qj.2815, 2016.

758   Poulsen, O. M., Breum, N. O., Ebbehoj, N., Hansen, A. M., Ivens, U. I., van Lelieveld, D., Malmros, P.,

759   Matthiasen, L., Nielsen, B. H., and Nielsen, E. M.: Sorting and recycling of domestic waste. Review

760   of occupational health problems and their possible causes., Sci. Total Environ., 168, 33–56, 1995.

761   Prospero, J. M. and Nees, R. T.: Impact of the North African drought and El Niño on mineral dust in the

762   Barbados trade winds, Nature, 320, 735–738, https://doi.org/10.1038/320735a0, 1986.

763   Randles, C. A., Sliva, A. M. da, Buchard, V., Colarco, P., Armenov, A., and Govindaraju, R.: The

764   MERRA-2 Aerosol Reanalysis, 1980 Onward. Part I: System Description and Data Assimilation

765   Evaluation, J. Clim., 30, 6823–6850, https://doi.org/10.1175/JCLI-D-16-0609.1, 2017.

766   Rayner, N. A., Parker, D. E., Horton, E. B., Folland, C. K., Alexander, L. V., Rowell, D. P., Kent, E. C.,

767   and Kaplan, A.: Global analyses of sea surface temperature, sea ice, and night marine air temperature

768   since the late nineteenth century, J. Geophys. Res. Atmos., 108, 4407,

769   https://doi.org/10.1029/2002jd002670, 2003.

770   Razakov, R. M. and Kosnazarov, K. A.: Dust and salt transfer from the exposed bed of the Aral Sea and

771   measures to decrease its environmental impact, in: The Aral Sea Basin, edited by: Micklin, P. P. and

772   Williams, W. D., Springer, Berlin, Heidelberg, 95–102, 1996.

773   Richon, C., Dutay, J., Dulac, F., and Wang, R.: Modeling the biogeochemical impact of atmospheric

774   phosphate deposition from desert dust and combustion sources to the Mediterranean Sea,

775   Biogeosciences, 15, 2499–2524, https://doi.org/10.5194/bg-2017-242, 2018.

776   Sabeerali, C. T., Ajayamohan, R. S., Bangalath, H. K., and Chen, N.: Atlantic Zonal Mode: An Emerging

777   Source of Indian Summer Monsoon Variability in a Warming World, Geophys. Res. Lett., 46, 4460–

4467, https://doi.org/10.1029/2019GL082379, 2019.

Sanchez de la Campa, A., Garcia-Salamanca, A., Solano, J., de la Rosa, J., and Ramos, J.-L.: Chemical and microbiological characterization of atmospheric particulate matter during an intense African dust event in Southern Spain., Environ. Sci. Technol., 47, 3630–3638, https://doi.org/10.1021/es3051235, 2013.

Schulz, M., Prospero, J. M., Baker, A. R., Dentener, F., Ickes, L., Liss, P. S., Mahowald, N. M., Nickovic, S., García-Pando, C. P., Rodríguez, S., Sarin, M., Tegen, I., and Duce, R. A.: Atmospheric Transport and Deposition of Mineral Dust to the Ocean: Implications for Research Needs, Environ. Sci. Technol., 46, 10390–10404, https://doi.org/10.1021/es300073u, 2012.

Singh, R. P., Prasad, A. K., Kayetha, V. K., and Kafatos, M.: Enhancement of oceanic parameters associated with dust storms using satellite data, J. Geophys. Res., 113, C11008, https://doi.org/10.1029/2008JC004815, 2008.

Srivastava, G., Chakraborty, A., and Nanjundiah, R. S.: Multidecadal see-saw of the impact of ENSO on Indian and West African summer monsoon rainfall, Clim. Dyn., 52, 6633–6649, https://doi.org/10.1007/s00382-018-4535-2, 2019.

Storch, H. von and Zwiers, F. W.: Statistical Analysis in Climate Research, Cambridge University Press, Cambridge, https://doi.org/DOI: 10.1017/CBO9780511612336, 1999.

Tegen, I., Lacis, A. A., and Fung, I.: The influence on climate forcing of mineral aerosols from disturbed soils, Nature, 380, 419–422, 1996.

Tokinaga, H., Richter, I., and Kosaka, Y.: ENSO Influence on the Atlantic Niño, Revisited: Multi-Year versus Single-Year ENSO Events, J. Clim., 32, 4585–4600, 2019.

Trenberth, K. E. and Hurrell, J. W.: Decadal atmosphere-ocean variations in the Pacific, Clim. Dyn., 9, 303–319, https://doi.org/10.1007/BF00204745, 1994.

Trenberth, K. E., Dai, A., Van Der Schrier, G., Jones, P. D., Barichivich, J., Briffa, K. R., and Sheffield, J.: Global warming and changes in drought, Nat. Clim. Chang., 4, 17–22, https://doi.org/10.1038/nclimate2067, 2014.

Veselovskii, I., Goloub, P., Podvin, T., Tanre, D., Da Silva, A., Colarco, P., Castellanos, P., Korenskiy, M., Hu, Q., Whiteman, D. N., Pérez-Ramírez, D., Augustin, P., Fourmentin, M., and Kolgotin, A.:

806   Characterization of smoke and dust episode over West Africa: Comparison of MERRA-2 modeling

807   with multiwavelength Mie-Raman lidar observations, Atmos. Meas. Tech., 11, 949–969,

808   https://doi.org/10.5194/amt-11-949-2018, 2018.

809 Wang, B., Wu, R., and Li, T.: Atmosphere-warm ocean interaction and its impacts on Asian-Australian

810   monsoon variation, J. Clim., 16, 1195–1211, https://doi.org/10.1175/1520-

811   0442(2003)16<1195:AOIAII>2.0.CO;2, 2003.

812 Wang, L., Chen, W., and Huang, R.: Interdecadal modulation of PDO on the impact of ENSO on the east

813   Asian winter monsoon, Geophys. Res. Lett., 35, https://doi.org/10.1029/2008GL035287, 2008.

814 Wang, S., Huang, J., He, Y., and Guan, Y.: Combined effects of the Pacific Decadal Oscillation and El

815   Niño-Southern Oscillation on Global Land Dry-Wet Changes, Sci. Rep., 4, 6651,

816   https://doi.org/10.1038/srep06651, 2014.

817 Watanabe, M. and Jin, F. F.: Role of Indian Ocean warming in the development of Philippine Sea

818   anticyclone during ENSO, Geophys. Res. Lett., 29, 1161–1164,

819   https://doi.org/10.1029/2001gl014318, 2002.

820 Watanabe, M., Shiogama, H., Tatebe, H., Hayashi, M., Ishii, M., and Kimoto, M.: Contribution of natural

821   decadal variability to global warming acceleration and hiatus, Nat. Clim. Chang., 4, 893–897,

822   https://doi.org/10.1038/nclimate2355, 2014.

823 Weare, B. C., Navato, A. R., and Newell, R. E.: Empirical orthogonal analysis of Pacific sea surface

824   temperatures, J. Phys. Oceanogr., 6, 671–678, 1976.

825 Weng, H., Ashok, K., Behera, S. K., Rao, S. A., and Yamagata, T.: Impacts of recent El Niño Modoki

826   on dry/wet conditions in the Pacific rim during boreal summer, Clim. Dyn., 29, 113–129,

827   https://doi.org/10.1007/s00382-007-0234-0, 2007.

828 Wu, R. and Kirtman, B. P.: Understanding the impacts of the Indian ocean on ENSO variability in a

829   coupled GCM, J. Clim., 17, 4019–4031, https://doi.org/10.1175/1520-

830   0442(2004)017<4019:UTIOTI>2.0.CO;2, 2004.

831 Wu, X., Liu, J., Wu, Y., Wang, X., Yu, X., Shi, J., and Bi, J.: Aerosol optical absorption coefficients at

832   a rural site in Northwest China : The great contribution of dust particles, Atmos. Environ., 189, 145–

833   152, https://doi.org/10.1016/j.atmosenv.2018.07.002, 2018.

834 Xi, X. and Sokolik, I. N.: Dust interannual variability and trend in Central Asia from 2000 to 2014 and

835   their climatic linkages, J. Geophys. Res. Atmos., 120, 12175–12191,

836   https://doi.org/10.1038/175238c0, 2016.

837 Yang, S. and Jiang, X.: Prediction of Eastern and Central Pacific ENSO Events and Their Impacts on

838   East Asian Climate by the NCEP Climate Forecast System, J. Clim., 27, 4451–4472,

839   https://doi.org/10.1175/JCLI-D-13-00471.1, 2014.

840 Yang, X. and Huang, P.: Restored relationship between ENSO and Indian summer monsoon rainfall

841   around 1999/2000, Innov., 2, 100102, https://doi.org/10.1016/j.xinn.2021.100102, 2021.

842 Yu, J.-Y., Mechoso, C. R., McWilliams, J. C., and Arakawa, A.: Impacts of the Indian Ocean on the

843   ENSO cycle, Geophys. Res. Lett., 29, 1204, 2002.

844 Yu, J. and Kao, H.: Decadal changes of ENSO persistence barrier in SST and ocean heat content indices :

845   1958 – 2001, J. Geophys. Res., 112, 1–10, https://doi.org/10.1029/2006JD007654, 2007.

846 Yu, Y., Notaro, M., Liu, Z., Wang, F., Alkolibi, F., Fadda, E., and Bakhrjy, F.: Climatic controls on the

847   interannual to decadal variability in Saudi Arabian dust activity: Toward the development of a

848   seasonal dust prediction model, J. Geophys. Res. Atmos., 120, 1739–1758,

849   https://doi.org/10.1002/jgrc.20224, 2015.

850 Yuan, Y. and Yang, S.: Impacts of Different Types of El Niño on the East Asian Climate: Focus on

851   ENSO Cycles, J. Clim., 25, 7702–7722, 2012.

852